crystals

MDPI

Review

Laser Floating Zone Growth: Overview, Singular Materials, Broad Applications, and Future Perspectives

Francisco Rey-García [1,*], Rafael Ibáñez [2], Luis Alberto Angurel [1], Florinda M. Costa [3] and Germán F. de la Fuente [1,*]

[1] Instituto de Nanociencia y Materiales de Aragón (CSIC-Universidad de Zaragoza), María de Luna 3, E-50018 Zaragoza, Spain; angurel@unizar.es
[2] Institut de Ciència dels Materials de la Universitat de València, C/ Catedrático José Beltrán, 2, E-46980 Paterna, Spain; Rafael.Ibanez@uv.es
[3] Departamento de Física & i3N, Campus de Santiago s/n, Universidade de Aveiro, PT-3810-193 Aveiro, Portugal; flor@ua.pt
* Correspondence: francisco.rey.usc@gmail.com (F.R.-G.); german.delafuente.leis@csic.es (G.F.d.l.F.)

Abstract: The Laser Floating Zone (LFZ) technique, also known as Laser-Heated Pedestal Growth (LHPG), has been developed throughout the last several decades as a simple, fast, and crucible-free method for growing high-crystalline-quality materials, particularly when compared to the more conventional Verneuil, Bridgman–Stockbarger, and Czochralski methods. Multiple worldwide efforts have, over the years, enabled the growth of highly oriented polycrystalline and single-crystal high-melting materials. This work attempted to critically review the most representative advancements in LFZ apparatus and experimental parameters that enable the growth of high-quality polycrystalline materials and single crystals, along with the most commonly produced materials and their relevant physical properties. Emphasis will be given to materials for photonics and optics, as well as for electrical applications, particularly superconducting and thermoelectric materials, and to the growth of metastable phases. Concomitantly, an analysis was carried out on how LFZ may contribute to further understanding equilibrium vs. non-equilibrium phase selectivity, as well as its potential to achieve or contribute to future developments in the growth of crystals for emerging applications.

Keywords: laser floating zone; laser-heated pedestal growth; single crystals; textured materials; congruent/incongruent melting

Citation: Rey-García, F.; Ibáñez, R.; Angurel, L.A.; Costa, F.M.; de la Fuente, G.F. Laser Floating Zone Growth: Overview, Singular Materials, Broad Applications, and Future Perspectives. *Crystals* **2021**, *11*, 38. https://doi.org/10.3390/cryst11010038

Received: 28 November 2020
Accepted: 29 December 2020
Published: 31 December 2020

1. Introduction

Growth of crystalline solids can be achieved by a large variety of methods driven by thermal or chemical potential gradients. Crystal growth in nature is achieved under many different geological conditions, in some cases under extremely high temperatures and pressure and in others by very slow solution processes [1]. Many current laboratory methods are nothing but transcripts of those that we can find in nature, as in the case of hydrothermal processes involved in the preparation of many functional materials [2]. A comprehensive classification of crystal growth techniques can be found in the classical work of Pamplin [3]. In this work, four main categories of growth methods are established: Growth from solid (S→S), melt (L→S), vapor (V→S), and solution (sol→S). Melt growth techniques are the choice methods to obtain bulk single crystals of inorganic materials and they could be divided into four categories: crystal pulling, directional solidification, floating zone, and Verneuil techniques [4]. Crystallization techniques such as Verneuil, Bridgman–Stockbarger, and Czochralski methods are usually employed for large and conventional production of gemstones (Al_2O_3 allomorphs and doped crystals, TiO_2, $SrTiO_3$), semiconductor single crystals (Si, Ge, GaAs), or metals (Pd, Pt, Ag, Au). In these methods, a material of approximately the correct composition is melted congruently, i.e., the crystalline phase is maintained before and after melting, being solidified in a carefully controlled fashion causing the formation of a single crystal from a well-oriented

seed material [5]. However, they present some disadvantages when the materials are highly refractory or exhibit incongruent melting. Likewise, they usually imply the use of a large amount of starting precursor materials, long processing times, and the use of crucibles that could introduce impurities on crystals with consequences in their physical properties. In contrast, the study of new materials implies limited quantities of precursors, the required highest purity possible to present the best performance, and, considering these competitive times, their production in the shortest time possible. Thus, the Laser Floating Zone (LFZ) technique, namely, Laser-Heated Pedestal Growth (LHPG), has been revealed as a suitable prototyping technique that enables the production of high-quality crystalline materials in a simple, fast, and crucible-free method with low consumption of precursor materials. In addition, several studies have allowed us to easily process materials presenting incongruent melting, as well as obtaining non-equilibrium phases.

The origin of this technique may be assigned to Haggerty in 1972 [6], who defined a Laser-Heated floating zone growth process of Al_2O_3 (sapphire) fibers for NASA (National Aeronautics and Space Administration; Cleveland, OH, USA). Feigelson later applied the method to the growth of single-crystal fibers with potential use in solid-state lasers [7]. A good number of materials have been obtained by LFZ since then, for a wide range of applications taking into account the continuous improvement of the technique along these years, considering both laser source and optical setup [7]. Thus, materials for photonics and electrical applications can be highlighted as the most produced by LFZ together with the industry interest on environmentally friendly processes and materials, reducing energy consumption and enhanced properties of materials. It must be noted that, since the reviews published by Feigelson in 1989 [7], Rudolph and Fukuda in 1999 [8], and Andreeta et al. in 2010 [9], there is no other review about materials processed by the LFZ (or LHPG) technique. Taking into account the materials produced during the past number of years, as well as the latest apparatus advances for enhancing the quality of the molten zone and the consequent solidification, this call for a review focused on the technique and its materials' development. Concomitantly, most promising fields are noted, highlighting the corresponding materials produced, aiming to define the future perspectives of the LFZ technique.

Before describing in detail the LFZ technique, focusing on materials developed for photonic or electrical applications, however, it is convenient to mention the analogous Optical Floating Zone (OFZ) technique [10–15]. In fact, a number of interesting papers have been published regarding the growth of different kinds of single-crystal materials. These include, for example, high-quality rubies [16], europium-doped, yttria-stabilized hafnia (YSH) [17], multifunctional $BaZrO_3$ [18], the $Ba_2PrFeNb_4O_{15}$ ferroelectric relaxor [19], or rare-earth disilicates of Er, Ho, and Tm with a rich range of interesting magnetic properties [20]. Technically, the difference between OFZ and LFZ is in the optical radiation sources used to attain heating and melting. Usually OFZ makes use of ellipsoidal mirrors with a secondary focal point at the center of the growing rod or crystal, while the primary focus contains a powerful halogen or xenon lamp. This setup allows achieving high melting temperatures with a significantly lower energy consumption, as compared to conventional crystallization methods described above [13,14]. However, the LFZ technique allows better control of the temperature gradient compared to OFZ, as well as higher temperatures [21] since the light focus in OFZ is broad and the temperature gradient at the interface between the solid and the liquid is less abrupt. This makes the melt seriously attack the feed rod and spill over to the crystal, eventually making the growth unstable [22]. Likewise, the use of lasers allows implementation of a high-strength metal growth chamber, permitting high pressures, up to 1000 bar [23]. Meanwhile, in conventional mirror-based designs, namely, OFZ chambers, apparently the maximum pressure achieved is in the proximity of 300 bar [15]. In both cases, high pressures are desired to enable the growth of highly volatile and metastable materials.

2. LFZ Technical Developments

The first equipment developed by Haggerty in 1972 [6] was proposed for the production at ambient atmospheres of Al_2O_3:Cr, TiC, and Y_2O_3 fibers, noting that there were no available crucibles for the melting of the first two materials. Thus, these materials were produced using an apparatus provided with a small 10-W CO_2 laser, coupled to a basic optical system composed of (1) the beam expanding and pointing optics, (2) the beam splitter, and (3) the beam splitting and focusing optical bench. The beam splitter consisted of a water-cooled, coated GaAs window and a front surface mirror. Meanwhile, the two furnace windows—after beam splitter—were made of NaCl. After that, beams were intercepted by semicircular and spherical mirrors and focused at the position of the molten zone. Finally, fiber withdrawal and feed-rod insertion mechanisms were installed inside the furnace as pulling heads.

Andreeta et al. [9] summarized the technical advances of existing prototypes through 2010. Among all advances, the introduction of the reflaxicon by Fejer et al. [24,25] may be highlighted. It enabled a circular, crown-shaped laser beam focus and, therefore, uniform radial heating. This term describes a setup of a two-stage pair of reflective linear axicon surfaces [21], which was invented by Martin in 1948 [26] and later improved by Nubling and Harrington in 1997 [27] (Figure 1). Likewise, processing under high-vacuum conditions, achieved for the first time by Brueck et al. in 1996 [28], must also be highlighted. Another remarkable advancement was achieved by Carrasco et al., in 2004 [29], through the application of an electrical current during processing. By establishing the Electrically Assisted Laser Floating Zone (EALFZ) (Figure 2) they demonstrated impressive preferential texture and the consequent enhancement in electrical properties of high Tc superconductors. In the same year and after previous experiments employing floating zone combined with a YAG ($Y_3Al_5O_{12}$) laser, Geho et al., in 2004 [30], reported the design of a hybrid laser floating zone machine for the successful growth of incongruently melting $Tb_3Al_5O_{12}$ (TAG) single crystals (Figure 3). This new device combined four CO_2 lasers and four halogen lamps, aiming to reduce temperature gradients during solidification. Likewise, Sekijima and Geho, in 2004 [31], patented an apparatus composed of two CO_2 lasers for growing TAG single crystals.

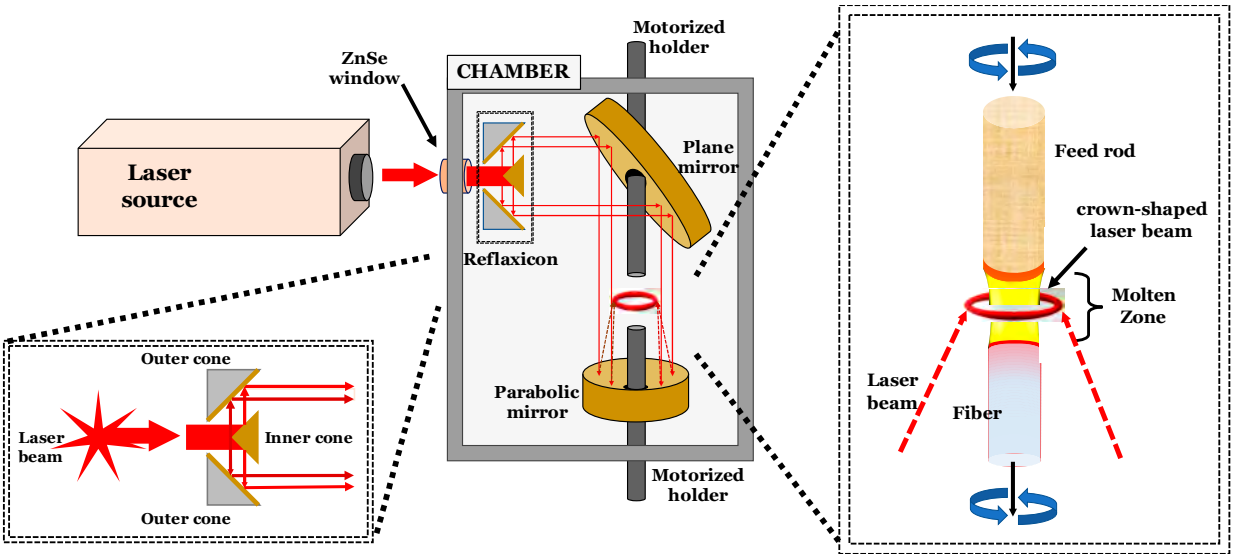

Figure 1. Schematic diagram of the typical Laser Floating Zone (or LHPG) setup, detailing both reflaxicon as molten zone area (see further details in [9,21]).

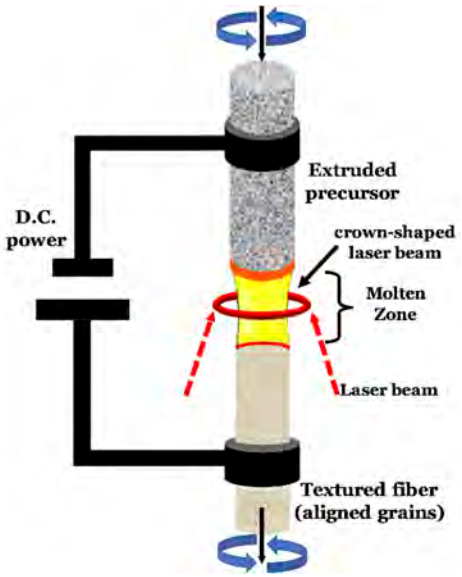

Figure 2. Schematic drawing of Electrically Assisted Laser Floating Zone (EALFZ) at the processing area, highlighting the D.C. power supply unit, Carrasco et al., 2004 [29].

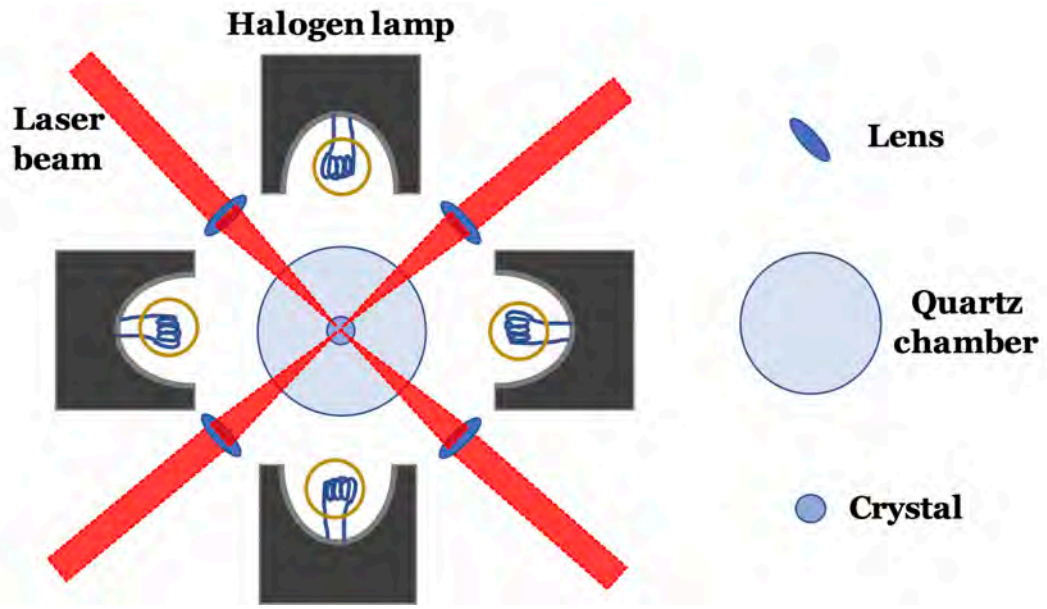

Figure 3. Top-view schematic drawing based on the hybrid Laser Floating Zone designed by Geho et al., in 2004 [30], and provided with four CO_2 lasers and four halogen lamps.

Outstanding advances were achieved during the last 10 years, also focused on improving radial heating uniformity. Most of these implied the use of laser diodes both to improve radial heating, envisaging the growth of incongruently melting materials, as well as to substantially increase total laser power. The first study was reported by Ito et al., in 2013 [22], who successfully grew incongruent materials such as $BiFeO_3$ and $(La,Ba)_2CuO_4$ by developing a laser–diode-heated floating zone (LDFZ) apparatus. The latter made use of five laser diodes emitting at a wavelength of 975 nm, with a total laser power output of 350 W and without use of a reflaxicon (Figure 4). In addition, these authors studied the effects of the number of laser diodes (3 to 8) on the quality of radial heating. A similar apparatus was recently employed by Kaneko NS Tokura, in 2020 [32], to grow refractory (Al_2O_3:Cr, SmB_6), incongruent melting ($Ba_2Co_2Fe_{12}O_{22}$) and volatile ($Nd_2Mo_2O_7$, $SrRuO_3$) materials by LDFZ, employing five laser diodes emitting at 940-nm wavelength with a total power

of 1 kW. Thus, the use of various lasers enables uniform irradiation intensity distribution on the periphery of the raw material. Moreover, a vertical irradiation intensity can be designed to exhibit a flat or bell-shape distribution to improve relaxation of residual thermal strain in the grown crystal [22,32]. Nowadays, the Crystal Systems Corporation (Hokuto, Yamanashi, Japan) commercializes a laser floating zone furnace that provides a total laser power output of 5 kW, employing five laser diodes emitting at a wavelength of 808 nm [33]. In addition, similar equipment from Quantum Design International (San Diego, CA, USA) allows monitoring the temperature in the range 1173–3273 K while achieving a maximum laser output power of 2 kW from five laser diodes [34].

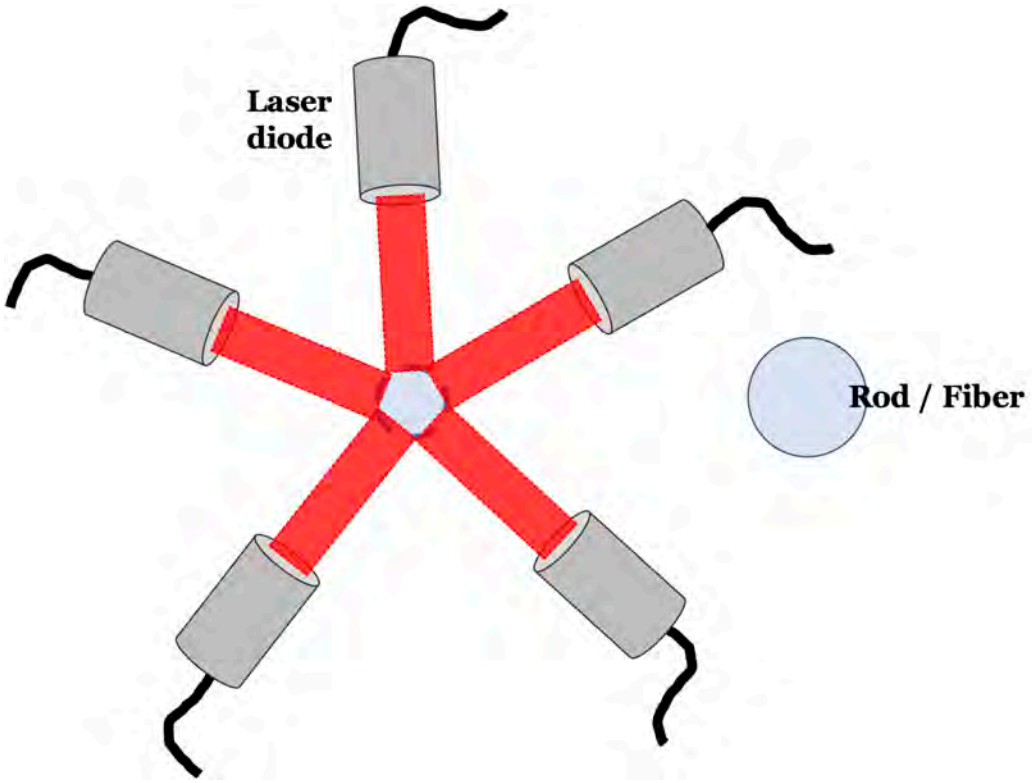

Figure 4. Top-view schematic drawing based on the Laser Diode Floating Zone (LDFZ) equipment designed by Ito et al., in 2013 [22], provided with five laser diodes, allowing a uniform irradiation intensity distribution on the periphery of the raw material [22,32].

Finally, Schmehr et al., in 2019 [23], developed a high-pressure LFZ (HP-LFZ) apparatus provided with seven laser diodes, emitting at a wavelength of 810 nm with a total laser output power of 700 W. They particularly aimed at avoiding outgassing/volatily effects inherent to materials that exhibit high vapor pressures at high temperatures. In addition, they also addressed the melting of highly refractory materials with volatile component loss reduction, by applying high processing gas pressures. Thus, Cu_2O, $Nd_2Zr_2O_7$, and $LiCuO_2$ crystals have been successfully grown using this last apparatus.

3. Experimental Procedure (Standard)

LFZ growth requires precursor powders in the form of cylindrical rods to be used as feed and seed and there are three typical processes to produce these precursor rods:

(1) The extrusion process is the most common way to prepare the precursor rod cylinders for the LFZ process, since it is a simple method, not requiring special equipment or additional hands [21,29]. Thus, the commercial raw oxide powders are mixed, according to the desired stoichiometry, and reduced in grain size with an agate ball mill or similar equipment. The purity of the precursors depends on the desired application. For example, the use of powders of 5–6 N of purity should be envisaged for

photonic applications. Aiming to bind the powder mixture for the extrusion process, polyvinyl alcohol (PVA, 0.1 g/mL) is added, mashing the powders until a compact and plastic paste is achieved. The obtained clay is then extruded into cylindrical rods, with diameters that can reach up to 5 mm, depending on the material's nature and its application. After extrusion, the cylindrical rods are dried in air and ready to be used as feed and seed materials (also known as green rods). However, it is important to emphasize that for support the extruded bars should have slots, aiming to guarantee their alignment during the drying process.

(2) Alternatively, single crystals or dense ceramics appropriately cut can also be used as seed or feed rods instead of green rods [26]. The use of bulk-grown crystal seeds favors the formation of single-crystalline fibers. This approach helps laser processing and allows enhancing the structural characteristics of the single-crystal fiber produced. Similarly, in the last 10 years, cladded, single-crystalline fibers, mainly used as amplifiers, have been produced from bulk crystal seeds covered by Sol-Gel or embedded into silica or borosilicate hollow tubes, among other coating approaches [35–39]. Furthermore, some works from Rutgers University (Piscataway, NJ, USA) reported the growth from Pt wires together with the use of seed crystals or presintered ceramics as feed rods [40–42].

(3) Likewise, precursor rods can be also prepared by cold isostatic pressing [43]. Through this compaction method, both mixed raw and presintered powders with the desired composition are enclosed in a flexible mold. This flexible bag is introduced into a perforated support inside a pressure container. Once this setup is sealed, fluid pressure is exerted over the outside surface of the container, allowing the container to press all around the bag and inducing uniform compaction of the powder and, consequently, a uniform density within the compacted rod [44].

The LFZ equipment usually comprises a CO_2 laser coupled to a reflective optical setup which includes a reflaxicon, described in the previous section. In the case of LDFZ, this optical setup is not present. Once seed and feed fibers are placed on the respective holders, a molten zone is formed by irradiating the densified rods with the CO_2 laser and a different optical configuration. Fibers can be grown in the ascending or descending direction from this molten region at a defined growth or pulling rate, in air or special atmospheres, depending on the materials' physico-chemical properties. Likewise, feed and seed rods should be rotated, favoring the mixing of precursors in the melt, homogenizing the temperature of the molten material, and contributing to reduce unsymmetrical thermal stresses. Concomitantly, occurrence of constitutional supercooling is reduced. Thus, the melt rotation stabilizes the heat and mass flow against undesirable temperature perturbations [45]. The growth process can end abruptly or by reducing the laser power gradually. This procedure is very important to reduce the thermal stresses and, therefore, to avoid crack formation [9,21].

4. Materials for Photonic and Optical Applications

Several high-quality crystals for photonic and optical applications have been obtained via the LFZ technique. These include laser garnets, luminescent, fluorescent, optoelectronic, and photorefractive materials. Indeed, Haggerty, in 1972 [6], produced ruby and yttria when the technique was reported. Likewise, Nd:YAG fibers were obtained by Stone et al., in 1976 [46], from a Nd:YAG preformed rod with a CO_2 laser. This was not the conventional LFZ method described here since a platinum wire was dipped into the melt and raised slowly to pull the desired crystal. The first notice about the production by LFZ (or LHPG) of crystals for laser applications was reported by Fejer et al., in 1984 [25], when the reflaxicon was introduced. The suitability of the LFZ apparatus developed was thus tested, producing sapphire, ruby, $LiNbO_3$, and Nd:YAG laser media.

Due to the crystal requirements for optics and photonics [47], defect-free, transparent, and highly pure materials with lower thermal conductivity [48] have been produced since the technique's origin [6]. An excellent compilation of active and passive photonic materials

was conveniently reported by Rudolph and Fukuda in 1999 [8]. Likewise, Maxwell et al., in 2017 [49], reported the LFZ production of neodymium- and ytterbium-doped single-crystalline YAG cylinders (SCF) with diameters under 1 mm and, in addition, processing in combination with the Sol-Gel method for obtaining cladded fibers. Moreover, the increasing interest of industry on efficient optical processes required an updated revision from that reported by Rudolph and Fukuda in 1999 [8]. Indeed, it is remarkable the great interest that has arisen recently on crystals for ultrashort pulsed laser systems [50,51] and for LED devices applied for indoor plants' growth [52], as a consequence of the increasing food requirements derived from the human population increase.

One of the most LFZ-developed materials is single crystal $Y_3Al_5O_{12}$ (YAG) as a laser medium. Despite the fact that it was produced by Fejer et al. in 1984 [25], a considerable amount of work has appeared during the last 20 years (Table 1) reporting its growth [35–38,40–42,49–51,53–72], improving the production efficiency [59,71], and also enhancing its mechanical and optical characteristics [38]. Among those studies, the work of Nie et al., in 2015 [37], who produced YAG single crystals doped with Er^{3+}, Ho^{3+}, Tm^{3+}, Nd^{3+}, and Yb^{3+} may be highlighted here. They studied the dopant distribution following the ideal concentration for optimal photonic properties, together with the enhanced mechanical and microstructural characteristics. Likewise, diode-pumped garnets based on YAG crystals doped with metallic ions such as Cr^{4+} for Q-switched laser operation were also developed [53,54]. Focusing on this composition, both Lai et al., in 2009 [60], and Yi et al., in 2010 [61], developed laser gain media and multi-pass ring laser devices, respectively, from single crystal fibers (SCF) with the double-clad structure. The double-clad structure fabrication has been generally achieved by covering the single-crystal fiber through Sol-Gel and later sintering [49] or basically inserting a diameter-reduced grown rod into silica- or glass-based capillary tubes [35,50,63,66,68]. These kinds of materials, namely, the cladded, single-crystal fibers, have been largely applied as fiber amplifiers of the laser radiation [40,67,70]. Recently, Kim et al., in 2019, produced Yb:YAG core/YAG-clad fibers by a three-step process, combining an initial growth of doped YAG fibers, followed by acid etching and, finally, an epitaxial hydrothermal growth of the undoped YAG cladding [72]. On the other hand, Ye et al., in 2005 [57], grew an excellent YAG:Cr^{3+} crystal to be used as a fiber thermometer. This was based on fluorescence lifetime and found applications in temperature monitors for microwave treatments and medium-voltage substations. This application for temperature sensing has been also successfully explored in work from Zhejiang University (Hangzhou, Zhejiang, China), reporting the growth of Y_2O_3:Er^{3+}/Yb^{3+} [73] and Y_2O_3:Ho^{3+}/Yb^{3+} [74] single-crystal fibers with up-conversion luminescent characteristics.

Other complex oxides have also been developed by LFZ. Harrington, in 2014 [42], reported, for example, the growth of single-crystal fiber garnets of $MgAl_2O_4$ (spinel) from commercial YAG seeds and Pt wires. In 2004, Romero et al. [75] produced multiwavelength-laser, single-crystal aluminates of $YAlO_3$ doped with Nd^{3+} (0.5–1.5 mol%). Recently, single crystals of orthosilicates (RE_2SiO_5) also doped with rare earths (RE) have been produced by LFZ two to three times faster than conventional methods like Czochralski [76–78], maintaining or even improving laser performance by doping with Nd^{3+} or Yb^{3+} [48]. Other typical garnets usually employed in commercial laser resonators are based on lanthanum vanadates. Such is the case for $LaVO_4$, $Gd_{1-x}La_xVO_4$, and $Y_{1-x}La_xVO_4$, produced by Andreeta et al. in 2006 [79] from mixtures of raw oxide powders. These were processed in air at relatively high growth rates (9–18 mm/h), as compared to those applied on Czochraslki. From the research group of Andreeta et al. (Universidade Federal de São Carlos; São Carlos, Brasil), erbium-doped and undoped $CaNb_2O_6$ and $CaTa_2O_6$ single crystals, suitable as laser active media, were also developed and produced [80]. The optically transparent $CaTa_2O_6$ single crystals were also grown by Almeida et al., in 2013 [81], exploring the three polymorphic modifications that this material exhibits at room temperature. Focusing on niobates, the production of promising optical active elements for lasers such as lithium niobates ($LiNbO_3$) [55,82–85] or incongruent melting lithium-potassium niobate ($K_3Li_{2-x}Nb_{5+x}O_{15+2x}$, KLN) [86–88] (Table 2) must be also high-

lighted. In addition, more niobates were also grown by LFZ for holographic devices, as photorefractive materials by doping with Fe [89,90], for nonlinear optics and acoustic wave devices [91], for wavelength and frequency modulators [92,93], and, in the case of the $EuNbO_4$, for optoelectronics as light emitters [94].

Table 1. $Y_3Al_5O_{12}$ (YAG) garnets grown by LFZ since the review by Rudolph and Fukuda in 1999 [8].

Year	Authors	Dopant	Application	Ref.
2000	Ishibashi & Naganuma	Cr^{4+}	Diode-pumped garnet	[53]
2002	Shen et al.	Cr^{4+}	Garnets for Q-switch lasers	[54]
		Nd^{3+}		
2003	Boulon et al.	-	Laser media	[55]
2003	Yoshikawa et al.	Yb^{3+}	Laser media	[56]
2005	Ye et al.	Cr^{3+}	Temperature sensor	[57]
2006	Bufetova et al.	Nd^{3+}	Laser media	[58]
2009	Chen et al.	-	Laser media	[59]
2009	Lai et al.	Cr^{4+}	Cladded Laser media	[60]
2010	Yi et al.	Cr^{4+}	Cladded Multi-pass ring laser	[61]
2011	Chang et al.	Cr^{3+}	Laser media	[62]
2011	Zhu et al.	-	Laser amplifier	[40]
2012	Lautsen & Harrington	-	Laser media	[41]
2012	Wang et al.	Cr^{4+}	Cladded fiber amplifier	[35]
2012	Kim et al.	Ho^{3+}	Cladded High power laser media	[63]
		Yb^{3+}	Cladded High power laser media	
2013	Hsu et al.	-	Cladded Laser gain media	[64]
2013	Hsu et al.		Multi-mode media	[65]
2013	Kim et al.		Cladded laser media	[36]
2013	Lai et al.	Cr^{4+}	Double-cladded fiber amplifier	[66]
2013	Maxwell et al.	Er^{3+}	Cladded laser media	[67]
		Nd^{3+}		
		Yb^{3+}		
2014	Harrington	-	Laser media	[42]
2014	Wang et al.	Nd^{3+}	Waveguide	[68]
2015	Nie et al.	Er^{3+}	Garnets	[37]
		Ho^{3+}		
		Nd^{3+}		
		Tm^{3+}		
		Yb^{3+}		
2016	Kim et al.	-	High power fiber lasers	[50]
		Ho^{3+}		
		Yb^{3+}		
2016	Oliete et al.	-	YbAG comparative study	[69]
2017	Liu et al.	Cr^{4+}	Fiber transmission systems	[70]
2017	Maxwell et al.	Er^{3+}	Laser performance of cladded-core	[49]
		Nd^{3+}		
		Yb^{3+}		
2019	Bufetova et al.	Er^{3+}	Laser media	[71]
2019	Kim et al.	Ho^{3+}	High power fiber lasers	[72]
		Yb^{3+}	High power cladded fiber lasers	
2019	Wang et al.	Yb^{3+}	High power laser	[51]
2020	Bera et al.	Nd^{3+}	Garnets	[38]
		Nd^{3+}/Ho^{3+}		

Following the production of laser garnets, gadolinium- and gallium-based compositions have also been produced during the last several years. Taking into account the ease of evaporation of gallium oxide (Ga_2O_3), an excess of the same must be introduced, aiming to obtain the desired compositions [95]. Thus, Harrington reported, for the first time in 2014 [42], the single-crystal production of $Gd_3Ga_5O_{12}$ (GGG) laser garnet. Recently,

Rey-García et al., in 2020 [21], produced, in air atmosphere, gadolinium oxyorthosilicate single crystals, suitable to be employed as laser host matrices.

Table 2. Niobates grown by LFZ since the review by Rudolph and Fukuda in 1999 [8].

Year	Authors	Material	Application/Study Aim	Ref.
2001	Reyes-Ardila et al.	$LiNbO_3$	LHPG technique development	[82]
2001	Matsukura et al.	KLN [1]	Optical applications	[86]
2002	Andreeta et al.	$LiNbO_3$	LHPG technique development	[83]
2003	Boulon et al.	$LiNbO_3$	Laser media	[55]
2003	Bourson et al.	$LiNbO_3$:Fe	Photorefractive material	[89]
2003	Cochez et al.	$LiNbO_3$:Fe	Photorefractive material	[90]
2004	Guo et al.	KLN [1]:Zn^{2+}	SHG [2] blue laser	[87]
2004	Nagashio et al.	$LiNbO_3$	Nonlinear optics and acoustic wave	[91]
2005	Chen et al.	$LiNbO_3$	Optical material growth & study	[84]
2005	Lee et al.	$LiNbO_3$:MgO	Wavelength modulator	[92]
2007	Chen et al.	$LiNbO_3$	Optical material growth & study	[85]
2008	De Camargo et al.	$CaNb_2O_6$	Laser media	[80]
		$CaNb_2O_6$:Er^{3+}	Laser active media	
2011	Maxwell et al.	KLN [1]	Laser media	[88]
2013	Graça et al.	$EuNbO_4$	Dielectric devices	[94]
2015	Kashin et al.	$LiNbO_3$	Frequency doubling	[93]

[1] KLN: $K_3Li_{2-x}Nb_{5+x}O_{15+2x}$. [2] SHG: second harmonic generation.

Typical sapphire (Al_2O_3), ruby (Al_2O_3:Cr), and rutile (TiO_2) crystals have been continually produced by this technique, improving both production efficiency and material properties, as can be deduced from work published in the last few years [22,23,32,39,42,96–104] (Table 3). Indeed, doping of sapphire with Cr^{3+} and Er^{3+}, or even codoping with Er^{3+}/Yb^{3+}, was achieved through LHPG by Seat in 2001 [96] and Seat and Sharp in 2003 [97], demonstrating the suitability of the fibers produced to be successfully employed for high-temperature sensing, as Ye et al., in 2005 [57], also similarly tested later for YAG:Cr^{3+}. Likewise, Lai et al. in 2016 grew borosilicate-cladded, single-crystalline-core sapphire fibers suitable to be employed in biomedical applications, such as light sources for endoscopy [39]. It must be highlighted that Lai et al., in 2018, also demonstrated a facile and scalable approach for the transformation of a centrosymmetric sapphire (α-Al_2O_3) crystal to a large-scale 3D metamaterial (Si^{4+}:γ-Al_2O_3) with sub-wavelength fine structures [104]. Coming back to garnets for laser operation and revising the work mentioned up to this point, we could metaphorically denote this section as "Laser Kindergarten: laboratories in those laser parents produced laser children". Additionally, due to their optical properties and their efficiency, it is also interesting to remark on the works focused on the growth of laser garnets based on disordered crystals like sesquioxides, fluorides, or chalcogenides (Table 4) [105]. Thus, the last 20 years have also witnessed the LFZ growth of crystals like Gd_2O_3 doped with Yb^{3+} [106], Lu_2O_3 doped with Yb^{3+} or Ho^{3+} [50,72,106], Sc_2O_3 [55], Y_2O_3 undoped and doped with Yb^{3+}, Er^{3+}, or Ho^{3+} [55,106,107], and Ta_2O_5 doped with Eu^{3+} [108], and fluorides like CaF_2:Yb^{3+} [109,110] or KY_3F_{10}:Yb^{3+} [22]. It must be highlighted that fluorides have been grown under Ar atmosphere.

Likewise, other complex oxides based on $2Al_2O_3$-SiO_2 (mullite), $Bi_4Ge_3O_{12}$ (BGO), or Lu_2SiO_5 (LSO) suitable to be used as scintillators have been grown in the last decade by this technique [111,112]. Visible light emission, highly efficient, solid-state, light-emitting materials allowing the fabrication of devices with low energy consumption, high brightness, and environmentally friendly characteristics, are presently of great interest for many researchers [52]. Thus, the LFZ or LHPG technique has allowed obtaining a wide production of phosphors and luminescent materials in the form of doped single crystals or polycrystalline and eutectic materials [52,73,74,112–115] in a fast manner. Despite this vast production, considering that this section is focused on single crystals applied as laser media

or other specific optical engineering applications, we will not delve into a topic that would probably need a chapter by itself.

Table 3. Sapphire (Al_2O_3) and ruby (Al_2O_3:Cr) fibers produced by LFZ since 1999 [8].

Year.	Authors	Material	Application	Ref.
2001	Seat	$Al_2O_3:Cr^{3+}$ $Al_2O_3:Er^{3+}$ $Al_2O_3:Er^{3+}:Yb^{3+}$	High temperature sensing	[96]
2003	Seat & Sharp	$Al_2O_3:Er^{3+}:Yb^{3+}$	High temperature sensing	[97]
2006	Liu et al.	Al_2O_3:Mg	Strengthened sapphire garnet	[89]
2010	Carvalho et al.	$2Al_2O_3$-$SiO_2:Nd^{3+}$	Scintillator	[111]
2012	Dragic et al.	Al_2O_3	Fiber sensors & high energy lasers	[102]
2012	Mesa et al.	Al_2O_3-ErAG [1]-ZrO_2	Selective emitter for Si TPV cells	[117]
2013	Ito et al.	$Al_2O_3:Cr^{3+}$	LDFZ technique development [2]	[22]
2014	Harrington	Al_2O_3	Laser media	[42]
2014	Lai et al.	$Al_2O_3:Ti^{4+}$	High power cladded fibers	[103]
2016	Lai et al.	$Al_2O_3:Ti^{4+}$	Light sources for endoscopy	[39]
2017	Bufetova et al.	Al_2O_3	Laser media	[100]
2017	Ren et al.	Al_2O_3-ErAG [1]-ZrO_2	Selective emitter for Si TPV cells	[116]
2018	Lai et al.	Si^{4+} : γ-Al_2O_3	Second Harmonic Generation	[104]
2019	Liu et al.	Al_2O_3	Laser media	[101]
2019	Schmehr et al.	$Al_2O_3:Cr^{3+}$	HP-LFZ furnace development [3]	[23]
2020	Kaneko & Tokura	$Al_2O_3:Cr^{3+}$	LDFZ technique development [2]	[32]

[1] ErAG: $Er_3Al_5O_{12}$; TPV: thermal photovoltaic cells. [2] LDFZ: Laser Diode Floating Zone. [3] HP-LFZ: High-Pressure Laser Floating Zone.

Table 4. Crystalline fibers of sesquioxides and other binary oxides produced by LFZ since 1999 [6].

Year	Authors	Oxide	Dopant	Application	Ref.
2001	Laversenne et al.	Gd_2O_3 Lu_2O_3 Y_2O_3	Yb^{3+} Yb^{3+} Yb^{3+}	Laser media	[106]
2002	Laversenne et al.	Y_2O_3	Er^{3+} Ho^{3+} Yb^{3+}	Laser media	[107]
2003	Boulon et al.	Lu_2O_3 Sc_2O_3 Y_2O_3	- - -	Laser media	[55]
2010	Saggioro et al.	Ta_2O_5	Eu^{3+}	Electro-optical applications	[108]
2012	Santos et al.	ß-Ga_2O_3	Eu^{3+}	Electro-optics (TCO) [1]	[95]
2012	Kim et al.	Lu_2O_3	Ho^{3+} Yb^{3+}	Laser media	[63]
2012	Rodrigues et al.	TiO_2	Cr^{3+}:Fe^{3+}	Electro-optics	[99]
2016	Kim et al.	Lu_2O_3	Ho^{3+} Yb^{3+}	Laser media	[50]
2019	Schmehr et al.	Cu_2O	-	Dye, fungicide, ...	[23]
2019	An et al.	Y_2O_3	Ho^{3+}:Yb^{3+}	Temperature sensing	[74]
2019	Bao et al.	Y_2O_3	Ho^{3+}:Yb^{3+}	Temperature sensing	[73]
2019	Kim et al.	Lu_2O_3	Ho^{3+} Yb^{3+}	Laser media	[72]

[1] TCO: Transparent Conductive Oxide.

Other interesting kinds of materials produced, as a response to the increasing energetic demand, are those in which the optical properties are modulated by electrons, namely, electro-optics. This, together with the previously commented gallium trend to be evaporated, make the work of Santos et al., in 2012 [95], scientifically very important. They were capable of growing fibers of the transparent conductive oxide (TCO) ß-Ga_2O_3 doped with Eu^{3+}, which is suitable to be employed on solar cell devices. Thus, bulk fibers were pro-

duced at relatively high speeds (10 to 30 mm/h) in air at atmospheric pressure from raw oxide powder mixtures of Ga_2O_3 and Eu_2O_3 with an excess of the former compound. More recently, Ren et al., in 2017 [116], grew polycrystalline $Al_2O_3/Er_3Al_5O_{12}/ZrO_2$ eutectic ceramics under a nitrogen atmosphere suitable to be used as selective thermal emitter for thermal photovoltaic (TPV) generation [117]. One year before, these researchers also grew Al_2O_3-$Yb_3Al_5O_{12}$ (YbAG) eutectic rods to be selective emitters for thermophotovoltaic (TPV) devices [69].

Following this study, one of the most remarkable advantages of this technique is the possibility to grow incongruent melting materials with relative ease and within short times. This way, an incongruent melting material, like TAG, suitable to be used as optical isolator, was successfully produced in a modified LFZ process. The latter entailed combining laser melting with four halogen lamps employed to reduce thermal gradients and favor TAG crystallization [30,31,118]. The first approach of this modified LFZ was presented by Sekijima et al., in 1999 [119], reporting the growth of cerium-doped $Y_3Fe_5O_{12}$ crystals (YIG) that can also be employed as optical isolators. Likewise, working on the LFZ apparatus development, Ito et al., in 2013 [22], were able to grow incongruently melting materials such as $BiFeO_3$ and $(La,Ba)_2CuO_4$, making use of a LDFZ apparatus that enables melting at moderate laser power values.

Finally, it is very important to highlight a couple of works reporting the LFZ growth of crystalline L-arginine phosphates (LAP), in essence, the production of crystalline structures of organic molecules [120,121]. Singh et al. in 2008 [120] reported the production of ~1-mm-diameter transparent crystalline fibers of rhodamine-6G (Rd6G)-doped L-arginine by LFZ, applying a very low laser power of 4 W at 36 mm/h growing speed over pressed rods of fully reacted precursor compounds. It is remarkable that despite the fact that LFZ is ideal for high-temperature melting materials, some authors have achieved crystalline growth for a material that presents weight losses starting at 473 K, with complete decomposition at about 523 K when it is grown by a solution crystallization method. Additionally, the fibers produced maintained transmission for up to four weeks, despite being stored without oil in normal laboratory conditions. A couple of years later, the same authors also produced other LAP crystalline fibers by LFZ [121]. Thus, potassium di-hydrogen phosphate (KDP)-doped L-arginine phosphate crystalline fibers were grown, applying ~5.4 W with a pulling speed of 194 mm/h. It must be noted that the optical quality of these phosphate crystalline fibers, however, is not comparable to those obtained for inorganic materials.

5. Materials for Electrical Applications

LFZ technique has been also extensively explored to produce materials for electrical applications, where metal oxide superconductors, thermoelectrics, and magnetic materials (Table 5) [122–157] particularly stand out. Indeed, LFZ is a recognized technique to grow textured materials due to the very localized heating that generates steep thermal gradients at the growth interface, keeping undercooling conditions for dendritic growth. This is particularly interesting to grow materials that exhibit crystalline structure where the growth rate is highly anisotropic. The directional growth (Figure 5), besides the favorable contribution of oriented grains to current transport, also contributes to reduce the number of grain boundaries, as the misaligned orientations are blocked during crystallization by the well-aligned dendrites [125]. Besides, it is well known that the solidification rate has a strong influence on the crystallization degree, particularly on the phase nature, size, and orientation of crystals. This is even more important in the LFZ growth, a non-equilibrium process (Figure 5) [9,126,127]. Bearing in mind the influence of the morphological characteristics on the transport performance, many studies were dedicated to the influence of growth rate on the fiber's microstructure [128,129], despite the fact that the optimum pulling rate also depends on the thermal gradients in the melt [130–132]. Moreover, with the growth conditions being far from equilibrium, multiphasic materials are usually obtained and, accordingly, many studies were dedicated to the effect of post-growth thermal treatment [133,134], as well as cation substitutions [135,136], among other effects.

Table 5. Materials for electrical applications since 1999 [8].

Year	Authors	Material	Tech. [1] Doping	Improved Properties/Results	Ref.
2008	Silva et al.	$La_{0.7}Ca_{0.3}MnO_3$	EALFZ/-	Field freezing, supercooling transition: planar to a cellular/dendritic S/L interface	[124]
2011	Amaral et al.	$CaCu_3Ti_4O_{12}$	LFZ/-	Dielectric properties single & polycrystalline CCTO [2]	[156]
2011	Sergeenkov et al.	$La_{0.7}Ce_{0.3}MnO_3$	LFZ/-	Three ferromagnetic transitions at 126 K, 180 K and 300 K	[157]
2012	Ferreira et al.	$Bi_2Ca_2Co_{1.7}O_x$	EALFZ/-	PF = 0.088 mW/K^{2}m @ 923 K	[123]
2013	Constantinescu et al.	$Bi_2Ba_2Co_2O_x$	LFZ/-	Grain alignment decrease secondary phases PF = 0.4 mW/K^{2}m @ 923 K	[141]
2013	Madre et al.	$Ca_3Co_4O_9$	LFZ/-	PF = 0.42 mW/K^{2}m @ 1073 K, (annealing 72 h)	[142]
2013	Sotelo et al.	$Bi_{1.6}Pb_{0.4}Sr_2Co_{1.8}O_x$	LFZ/Pb & Ag	PF = 0.42 mW/K^{2}m @ 923 K (3wt% Ag)	[143]
2014	Rasekh et al.	$Bi_2Ca_2Co_{1.7}O_x$ + $Ca_3Co_4O_9$	EALFZ/-	PF = 0.18 mW/K^{2}m @ 298 K PF = 0.3 mW/K^{2}m @ 923 K, samples grown at 300 mA	[147]
2016	Madre et al.	$Bi_{2-x}Pb_xBa_2Co_2O_y$	LFZ/Pb	ZT = 0.53 @ 650 °C, 0.2 Pb-doped	[136]
2017	Madre et al.	$Bi_{1.6}Pb_{0.4}Ba_2Co_2O_y$/Ag	LFZ/Ag	PF = 0.46 mW/K^{2}m @ 923 K (annealed)	[146]
2018	Çetin Karakaya et al.	$Bi_2Sr_2Co_2O_y$	LFZ/Na	Grain alignment decrease secondary phases	[144]
2018	Ferreira et al.	$BaFe_{12}O_x$	LFZ/-	Fe_2O_3 and $BaCO_3$ precursors: high abundance and low costs	[155]
2019	Ferreira et al.	$CaMnO_3$	LFZ/-	PF = 0.39 mW/K^{2}m @ 1073 K, (10 mm/h)	[154]
2019	Ferreira et al.	$Ca_{0.9}La_{0.1}MnO_3$	LFZ/La	(no data)	[154]
2019	Ferreira et al.	$CaMn_{0.93}Nb_{0.05}O_3$	LFZ/Nb	(no data)	[154]
2019	Özçelik et al.	$Bi_2Sr_2Co_2O_y$	LFZ/K	Grain orientation decrease secondary phases ZT = 0.029 @ 400 K (x = 0.10)	[145]
2020	Carreira et al.	$Ca_{1-x}Pr_xMnO_3$	LFZ/Pr	PF = 0.303 mW/K^{2}m @ 1123 K for (100 mm/h, air, annealing 1573 K)	[153]
2020	Ferreira et al.	$Bi_2Sr_2Co_{1.8}O_y$	EALFZ/-	Grain orientation decrease secondary phases ZT = 0.09 @ 923 K (+300 mA)	[148]

[1] Tech.: Technique employed. [2] CCTO: $CaCu_3Ti_4O_{12}$.

In the last decade, thermoelectric (TE) materials have been intensively explored by LFZ. This is because they have attracted huge attention as a very promising technology, considering their energy-conversion ability. Thermoelectric materials can directly transform heat energy into electrical power as a consequence of the well-known Seebeck effect. The transformation of a thermal gradient into electrical energy enables waste heat recovery and reduction of CO_2 production. Nowadays, the commercial applications are based on alloys and/or intermetallic materials, with high thermoelectric performances at relatively low temperatures. However, there are many limitations for their use in several applications, such as their low abundance, high costs, toxic nature, and their relatively low working temperatures associated to their intrinsic thermal degradation. These limitations were overcome by the discovery of thermoelectric properties in $Na_2Co_2O_4$ [137]. This material can work at high temperatures in ambient atmosphere conditions and is free of heavy or

toxic elements. Following this discovery, great efforts were made to find similar characteristics materials. Other oxides, such as Ca-Co-O, Bi-Sr-Co-O, or Bi-Ca-Co-O, with attractive thermoelectric properties were thus studied [138,139]. These layered cobaltite materials exhibit a strong crystallographic anisotropy and tend to crystallize with stacked plate-like grains, a suitable structure to be explored by a directional growth. Following this idea, the LFZ growth without and with applied electrical current (EALFZ) was executed, aiming to increase the preferential grain orientation and to produce ceramics with very high density to reduce electrical resistivity and, consequently, raise their thermoelectric performance (Figure 5).

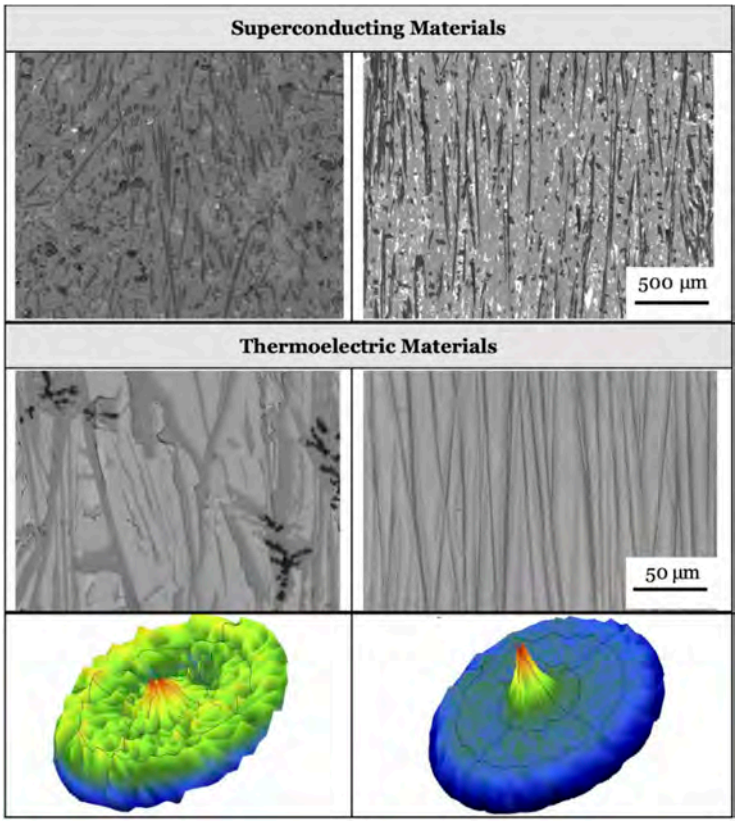

Figure 5. Micrographs performed on longitudinal polished sections of superconducting ($Bi_2Sr_2CaCu_2O_x$) and thermoelectric ($Bi_2Ca_2Co_{1.7}O_x$) materials grown by LFZ (**left**) and EALFZ with 300 mA (**right**). Pole figures of cross sections of the thermoelectric samples highlight the beneficial effect of the electrical current application on the grain alignment during the crystallization process (adapted with permission [147], Copyright 2014, Elsevier).

Among the several studies carried out in p-type ceramic oxides, it is important to emphasize the work performed by Sotelo and co-workers (INMA, Instituto de Nanociencia y Materiales de Aragón; Zaragoza, Spain) that extensively explored the effect on thermoelectric performances of growth and annealing conditions [141,142], doping and co-doping [136,143–145], and composites' formation [146] (Table 5). All textured samples prepared by LFZ showed remarkable increase of power factor (PF) values as compared with conventional, sintered ceramics due to the preferential grain alignment along the growth axis. Nevertheless, it is important to emphasize the high amount of secondary phases that is usually produced due to the incongruent melting behavior of these oxide materials, as well as the generation of oxygen vacancies associated to the fast solidification process [142]. The optimization of microstructural characteristics through the growth and annealing conditions are reflected in the thermoelectric performance, with a significant increase in the PF values, reaching much higher values than the ones typically obtained in misfit cobaltites

processed by conventional solid-state reaction [141,142]. The highest power factor values (0.42 mW/K^{2}m at 923 K) observed for $Ca_3Co_4O_9$ are a consequence of phase content, high apparent density, grain alignment, and Co^{3+}/Co^{4+} relationship [142]. The thermoelectric performance of misfit cobaltites can be controlled not only by the grain orientation but also by cation substitutions. Following this approach, many dopants were studied in the CoO-based families, namely, by Pb incorporation [136,143–145]. An important improvement on the resistivity and thermopower was obtained for $Bi_{2-x}Pb_xCa_2Co_{1.7}O_y$ with 0.4 Pb substitution [143]. Likewise, exposing the as-grown samples to a post-annealing step induced an increase of thermoelectric phase content and, consequently, an improvement in PF by a factor of two at room temperature [136]. The thermal conductivity of these samples was measured and an estimated ZT value of 0.53 for the 0.2 Pb-doped samples was obtained, which is much higher than the ones reported in the literature [136]. The effect of K aliovalent substitution for Sr on the $Bi_2Sr_2Co_2O_y$ system enabled an increase in ZT values up to 0.10 of K-content, reaching 0.029 at around 400 K, pointing to a positive effect on the formation of a spin-density wave state when K substitutes Sr in the crystalline structure [136]. Considering the importance of electrical connectivity through the grain boundaries on thermoelectric properties, the addition of metallic Ag was explored [143,146]. The performance was significantly improved after post-thermal treatment optimization (3 wt% Ag annealed samples at 923 K, 24 h), reaching a PF value of 0.32 mW/K^{2}m at 1023 K [146].

Considering the excellent results obtained when an electrical current was applied during the crystallization of superconducting materials using the EALFZ method [122], the same approach was explored by the group of Costa et al. (Universidade de Aveiro; Aveiro, Portugal) in p-type TE materials, considering the similarity of both types of crystalline structures [123,147,148] (Table 5). The current application in the EALFZ strongly modified the phase development, the crystal morphology, and the grain alignment [29,124]. If a direct current (DC) is applied, by connecting the positive and negative poles, respectively, to the seed and feed rod samples, the system approaches equilibrium, since it drastically changes the solidification features, namely, the solute ion distribution, phase nature, and crystal growth kinetics [29,123,124,148]. These modifications arise from the electromigration phenomena introduced by the electrical current application during the growth process [29]. Consequently, the ion flux follows on the balance of the constitutional undercooling and the electromigration effect. Accordingly, this electrical field through the solid–liquid interface accelerates the solute ions until a drift velocity is reached. Thus, the effective segregation coefficient (the solute ratio concentrations in the crystallized solid at the level region and in the bulk liquidus) is significantly modified [29,127,149]. An equivalent phenomenon was observed in other systems when an electric current was applied, namely, the refinement of Bi-Sn and Au-Ge alloys [149,150].

The polarity effects of an external current applied during the growth process (EALFZ) was investigated in the $Bi_2Ca_2Co_{1.7}O_x$ system [123]. A significant improvement of power factor was obtained for samples grown with the positive pole connected to the seed rod, around 50% higher than those measured on samples grown by LFZ but without current application. The main reason for this improvement was the grain orientation and the crystal size of the thermoelectric phase. In contrast, the reverse current (negative electrode connected to the seed rod) favors the non-thermoelectric phase's development. The same behavior was observed in $Bi_2Sr_2Co_{1.8}O_y$, with the best thermoelectric performances obtained for samples grown under +300 mA, reaching a ZT value of 0.09 at 923 K [148]. Exploring the same technique, a new thermoelectric composite was successfully grown by EALFZ with a 300 mA applied current, promoting the formation of $Bi_2Ca_2Co_{1.7}O_x$ + $Ca_3Co_4O_9$ thermoelectric phases (Figure 5) [147]. Under these conditions the Seebeck coefficient is higher than that obtained for single crystals due to the formation of oxygen vacancies and PF values of 0.18 mW/K^{2}m at room temperature and 0.3 mW/K^{2}m at 923 K being obtained, which are the highest reported values for $Bi_2Ca_2Co_{1.7}O_x$ polycrystalline materials.

TE devices are made by joining at least two semiconductor materials together (TE module), one n-type (negative thermopower and electron carriers) and the other p-type (positive thermopower and hole carriers), wired electrically in series and thermally in parallel. This way, in addition to the development of p-type materials, n-type oxide materials have also been explored in the last decade. Transition metal oxides are gaining increasing attention for their TE properties due to their high thermal stability and tunable electronic and phonon transport properties. Among the n-type materials, $SrTiO_3$, $CaMnO_3$, and ZnO are the best candidates for TE power-generation modules operating at mid- to high-temperature ranges [151]. The high values of their Seebeck coefficients arise from either high carrier effective masses due to electronic correlations or from electron–electron interactions [152]. In the case of calcium manganite-based thermoelectrics, among the materials processed by conventional routes, Pr substitution shows high ZT values [152]. Accordingly, Pr-substituted calcium manganite was selected as a model system to study the relevant impacts of LFZ processing under different growth atmospheres on the thermoelectric performance [153]. Also, Nb and La were explored [154], putting in evidence that PF is significantly affected by the growth conditions and that additional heat treatment of the laser-processed fibers could improve TE performance. The guidelines suggest that LFZ is a suitable technique for processing thermoelectric perovskite-type manganites requiring, however, an optimization of growth and thermal annealing conditions (Table 5).

Recently, a new thermoelectric material composed of environmentally friendly elements, with nominal $BaFe_{12}O_x$ composition, was also processed by LFZ [155] (Table 5). Its highest power factor measured at 1073 K (0.2 mW/K^2m) is comparable to the best observed so far in oxide ceramic materials, with additional advantage of high abundance and low costs of Fe_2O_3 and $BaCO_3$ precursors.

LFZ was explored also to produce other materials for electrical applications, taking advantage of the LFZ ease to produce single crystals and polycrystalline ceramics. Thus, aiming to better understand the main mechanisms of the colossal dielectric constant of $CaCu_3Ti_4O_{12}$ (CCTO), several samples were grown by LFZ under different growth conditions [156] (Table 5). The results suggest that a polarization mechanism is present and should contribute toward a further increase of the dielectric constant. Moreover, the dielectric properties of this perovskite-structured material measured at microwave frequency (2.7 GHz) by the resonant cavity method confirm the high dielectric constant (56.7) and relatively low values of tan δ (0.04), putting in evidence that this material is potentially interesting for microwave device applications.

The LFZ technique was also used to produce manganites of $La_{0.7}Ce_{0.3}MnO_3$ (LCMO), a fascinating material that exhibits colossal magnetoresistance due to the presence of the mixed valence of manganese as Mn^{3+} and Mn^{4+} [157] (Table 5). The magnetic properties of the LCMO fibers grown by LFZ were evaluated and three ferromagnetic transitions were detected at 126, 180, and 300 K. The possibility to synthesize bulk electron and hole doped manganites by LFZ will have a significant impact on designing new hybrid devices that take advantage of both spin and charge degrees of freedom. As referred above, one of the major effects of the EALFZ technique is the control of the effective distribution coefficients, which approximate to the equilibrium coefficient values when the current is applied [29]. This field-modified segregation effect was demonstrated in perovskite-based manganese oxides ($Ln_{0.7}Ca_{0.3}MnO_3$) with colossal magnetoresistive (CMR) effect [121]. Indeed, the application of an electric field decreased the macrosegregation phenomenon, even at low cooling rates. A transition of planar to a cellular solid–liquid interface due to constitutional supercooling conditions due to field freezing effects was observed. Uda and co-workers (Institute of Materials Research, Tohoku University; Japan) also imposed an external electric field during oxide crystal growth, putting in evidence that it is possible to change an incongruent solidification into a congruent one [158]. The same behavior was observed in the case of $La_3Ga_5SiO_{14}$, as well as in $LiNbO_3$, due to the modifications of chemical potentials under the extrinsic electric field. In addition, the group of T. Duffar (University of Grenoble;

Grenoble, France) put in evidence recently a significant modification of the eutectic phase diagram induced by an external field for the Al_2O_3-YAG-ZrO_2:Y system [159].

6. Materials for Applications in Superconductivity

As introduced in the previous section, texturing has been promoted in high-temperature superconducting materials, aiming to enhance superconductivity. The development of power applications based on these materials compel strong requirements on these anisotropic materials. This is more evident for the Bi-Sr-Ca-Cu-O families because of their small coherence length and a large crystallographic cell that are responsible for an extreme two-dimensional behavior. Traditional ceramic processing technologies are not adequate for obtaining bulk materials with the minimum level of performance in order to be used in large-scale electrical applications.

Early works were carried out in the $YBa_2Cu_3O_x$ system using CO_2 lasers as heat sources [160–163]. These initial works showed that LFZ processing is not an adequate technique to obtain textured rods with high critical current values. Apart from the fact that a substantial evaporation takes place when Y_2O_3, $BaCO_3$, and CuO are used as precursors, it was observed that the directional solidification process was performed using a semisolid zone instead of a complete molten zone, due to the peritectic reaction that controls solidification in this material. In all the cases, growth rates lower than 40 mm/h were required to maintain a stable growth habit and the process had to be performed in controlled atmospheres, usually with oxygen partial pressures in the range between 6 and 10^3 Pa.

Different studies showed that the Bi superconducting phases were more appropriate for using LFZ as a texturing technique, because they exhibit high stability during incongruent melting and low evaporation and very low deviations from the material stoichiometry [160,164–168]. LFZ produces a conglomerate of crystals with their crystallographic c-axis perpendicular to the sample growth direction, and the a-b planes aligned in the direction of the fiber axis, improving electrical transport current flow [125]. Bi superconductors present two phases with critical temperatures above 77 K: $Bi_2Sr_2CaCu_2O_{8+\delta}$ (Bi-2212) with $T_c \approx 80$ K and $Bi_2Sr_2Ca_2Cu_3O_{10+\delta}$ (Bi-2223) with $T_c \approx 110$ K.

The Bi-2223 phase has lower stability and, despite greater interest due to its higher critical temperature, it was very complicated to obtain textured materials with this composition. Initial works [167,169,170] explored the strategy of substituting some amount of Bi by Pb and the LFZ process was performed in an 8% O_2 in Ar mixture flowing through the growth chamber. In the textured material, the main phase is the Bi-2212 phase and additional annealing is required to partially recover the Bi-2223 phase. Due to the high density of the textured materials obtained by LFZ, this annealing was longer in comparison with ceramic pellets. A second alternative was to modify the stoichiometry of the precursors aiming to enhance the formation of the Bi-2223 phase. Larrea et al., in 1994 [171], used the $Bi_{1.87}Pb_{0.35}Sr_{1.87}Ca_4Cu_6O_y$ composition adding an extra amount of Ag. Costa et al. proposed the use of $Bi_2Sr_2Ca_2Cu_4O_{11}$ [125,133] and Miao et al., in 1997 [172], proposed precursors with different proportions of Bi-2212, $Bi_2Sr_2CuO_6$ (Bi-2201) and $CaCuO_2$.

Due to the higher stability of the Bi-2212 phase, an important amount of work reported was focused on this phase [132,135,164,168,173–183]. During these works, the Nd:YAG radiation started to be used as an alternative to the CO_2 lasers [168,175], observing that, with similar focusing optics, 1.06-μm radiation is more adequate to process textured Bi-2212 superconductors because these oxides absorb the 10.6—μm radiation mostly in the surface, creating larger radial temperature gradients and larger radial inhomogeneities due to constitutional supercooling. These studies [125,173,174,177] showed that in as-grown samples, the superconducting phase only develops for thin samples ($\Phi < 250$ μm) and with very low growth rates (<5 mm/h). When the growth rate increases, growth is dominated by constitutional supercooling. Under these conditions, the first solid phases formed during solidification are Sr-Ca-Cu oxides, normally the (Sr,Ca)CuO_2 (1/1 phase) and, in some cases, the $(Sr,Ca)_{14}Cu_{24}O_{41}$ (14/24 phase), and the melt becomes enriched in Bi_2O_3, generating some superconducting grains with intergrowths of the Bi-2212 and

the Bi-2201 phases and an amorphous matrix of frozen bismuth-rich liquid phase between them. The growing habit of the 1/1 phase has the b-axis parallel to the growing direction and the c-axis along the shorter dimension in the transverse cross section [125] and this determines the texture of the superconducting material. Size and radial distributions of these phases are strongly dependent on the thermal gradients induced during the LFZ process and they can be controlled by adjusting the processing parameters, mainly the growth rate [177], the laser power, or the initial precursor stoichiometry [178]. The strong correlation between the effects of the different processing parameters complicates the optimization process. A Simplex optimization method was proposed [179] to process, at the same time, four growth parameters (laser power, the growth rate, and the precursor and textured rod rotation speeds) and four annealing parameters, taking as control variables to obtain high critical current values and short processing times. Main conclusions of the optimization process are that high laser powers originate drastic reductions in the T_c values of the superconducting grains that grow within the central part of the rod. The second main conclusion is that a two-step annealing is needed. During the first step, at 1143 K, cation diffusion takes place to form the superconducting phase. In the second one, at 1073 K, the oxygen content required to optimize the critical temperature value is established. Critical current densities of the order of 5500 A/cm^2 at 77 K in 1-mm-diameter rods were reached after these optimization studies. Also, it was observed that critical current values decreased linearly with sample diameter, with the magnetic field generated at the sample surface being the limiting factor.

Several works have analyzed the influence of modifying the composition of the Bi-2212 precursor in the final microstructure of the textured material. Results showed that moderate Ag additions, with contents up to 3 wt%, reduce porosity and increase electrical connectivity because Ag fills the holes between superconducting grains [180]. Also, the substitution of some cations has been explored. For instance, Ca substitution by Y ions [181] generates an increase in the critical temperature values but with a deterioration of the grain alignment, while substitution by Rb [182] or Cs [183] leads to an increase of the pinning force at 10 K by about 20%.

Aiming to increase the level of current that can be transported by these materials, some studies have been performed, aiming to increase the cross section of the textured material. Vieira et al., in 2012 [130], analyzed the thermal gradients induced in rods with diameters between 1.75 and 2.5 mm and how they affect the phase distribution in the cross section of the sample and in the superconducting properties. Natividad et al., in 2001 [184], used LFZ to induce texture in hollow cylinders with external diameters up to 10 mm. The external part of the cross section is similar to that observed in bulk samples. These samples were used to fabricate a current lead with a coaxial configuration, showing an increase in the critical current value due to the reduction of the generated magnetic fields. Laser power limits the maximum thickness of the hollow cylinder. Angurel et al., in 2009 [185], proposed a new alternative with the aim to be able to texture rods with any diameter. In this case, samples are placed on a support that contains a series of Al_2O_3 rods in constant rotation, on top of which superconductor cylinder preforms are placed. The proposed laser system was a diode laser and allowed to process several pieces in parallel.

As it has been mentioned in previous sections, the group from Universidade de Aveiro (Costa et al.) introduced a modification in the LFZ process, called EALFZ, in which a DC electrical current is applied through the solid–liquid interface during the solidification process [29,122,127,128,134,186,187]. This modification was applied to the Bi-2212 and to the Bi-2223 phases, showing excellent results in both cases. When the electrical field is applied in the direct polarization configuration (positive pole connected to the seed) solidifications deviate from metastability and the primary solidification phase is mainly the 14/24 phase, yielding thinner and longer grains in the as-grown material and an improved texture in the superconducting rod. By contrast, when a reverse polarization is used, the dendritic microstructure disappears, generating a globular structure. Applying an

electrical current of 300 mA in the processing of Bi-2212/2.9 wt% Ag rods, it was possible to reach critical current values at 77 K of the order of 5800 A/cm^2 in samples of 2.3 mm in diameter, ~2.5 times higher than the values measured in similar samples processed without applying the electrical current during the solidification [122]. A review of the evolution of the superconducting families and the wavelength of the lasers used to process these materials is presented in Table 6.

Table 6. Superconducting materials produced by LFZ.

Year	Authors	Material [1]	Laser	Ref.
1988	Feigelson et al.	Bi-2212	CO_2	[164]
1989	Qiao et al.	YBaCuO, Bi-2212	CO_2	[160]
1989	De la Fuente et al.	Bi-2223	CO_2	[166]
1989	Carillo-Cabrera et al.	Bi-2223	CO_2	[169]
1989	Gazit et al.	Bi-2212	CO_2	[173,174]
1992	Cima et al.	YBaCuO	CO_2	[161]
1992	Snoeck et al.	Bi-2223	CO_2	[170]
1994	Figueredo et al.	YBaCuO	CO_2	[162]
1994	Larrea et al.	Bi-2223	CO_2	[171]
1995	De la Fuente et al.	Bi-2212, Bi-2223	CO_2, Nd:YAG	[175]
1997	Costa et al.	Bi-2223	CO_2	[123]
1998	Diez et al.	Bi-2212, Bi-2223	Nd:YAG	[176]
1998	Angurel et al.	Bi-2212	Nd:YAG	[177]
1999	Costa et al.	Bi-2223	CO_2	[133]
2004	Carrasco et al.	Bi-2223	Nd:YAG	[29]
2004	Costa et al.	Bi-2223	Nd:YAG	[186]
2004	Natividad et al.	Bi-2212	Nd:YAG	[179]
2005	Sotelo et al.	Bi-2212	Nd:YAG	[180]
2015	Costa et al.	Bi-2212	CO_2	[122]
2016	Özcelik et al.	Bi-2212	Nd:YAG	[181]
2020	Özcelik et al.	Bi-2212	Nd:YAG	[182]

[1] YBaCuO: $YBa_2Cu_3O_{7-\delta}$; Bi-2212: $Bi_2Sr_2CaCu_2O_{8+\delta}$; Bi-2212: $Bi_2Sr_2Ca_2Cu_3O_{10+\delta}$.

These superconducting materials were used in the development of the superconducting part of current leads [188]. In the framework of a collaboration between the INMA, the CEDEX-CIEMAT Laboratory of Applied Electromagnetics (CEDEX: Centro de Estudios y Experimentación de Obras Públicas, CIEMAT: Centro de Investigaciones Energéticas, Medioambientales y Tecnológicas; Madrid, Spain) and the company ANTEC (Antec Inc.; Freemont, CA, USA), the company designed and fabricated a set of 600-A current leads for the LHC (Large Hadron Collider) correction magnets at CERN (European Organization for Nuclear Research) [189,190]. Each module consisted of four Bi-2212 textured bars, with a diameter of approximately 0.8 mm, connected in parallel. The module has to work at temperatures close to 50 K, in which the expected critical current can reach values close to 1200 A. This requirement revealed that one of the main limitations to developing technological applications with these materials was to obtain good electrical contacts to inject the electrical current. This called for an effort to deposit on the oxide surface a stable, uniform, and reproducible metal layer. Painting, sputter deposition, or electrodeposition processes from non-aqueous solvents [191] have been used. In all the cases, best results were obtained when the coating was fabricated in the as-grown material and the annealing of the superconducting rod was used to consolidate the electrical contact. Reproducible surface contact resistivity values lower than 10^{-9} Ω cm^2 were reached, values that allow us to use these materials in electrical applications where high transport currents are required.

7. Incongruent Melting and Volatile Materials for Additional Applications

Researchers working on LFZ have shown every so often the possibility to obtain incongruent melting materials in a more or less controllable, direct, and fast way. In most cases, this was possible thanks to high temperatures provided within controlled atmo-

spheres and fast speeds. Lately, as was mentioned in Section 2, equipment setup advances providing high-pressure [23] or uniform radial heating by using various laser diodes [22,32] has allowed us to synthesize volatile (Li_2CuO_2, $Nd_2Mo_2O_7$, $SrRuO_3$) and incongruent melting ($BiFeO_3$, $(La,Ba)_2CuO_4$, $Ba_2Co_2Fe_{12}O_{22}$) materials. For example, Schmehr et al., in 2019 [23], were able to grow volatile Li_2CuO_2 by introducing a 80:20 Ar:O_2 atmosphere with a total pressure of 98.69 atm (100 bar) for avoiding volatility. In contrast, the absence of special atmospheres when processing an incongruent melt system like Nd_2O_3:SiO_2 has allowed us to synthesize unexpected materials. Thus, from stoichiometric mixtures of Nd_2O_3 and SiO_2 processed in air, a biphasic Nd_2SiO_5:$Nd_{9.33}(SiO_4)_6O_2$ material has recently been produced by Rey-García et. al., observing how the dielectric character of the stoichiometric phase rules electrical properties, making it suitable for microwave dielectric devices [192]. Likewise, for growing crystals of the pyrochlore-type $Nd_2Mo_2O_7$ (NMO), suitable for Hall effect sensors, only a slight pressure of 1 atmosphere is needed, as recently reported by Kaneko and Tokura, in 2020 [32], to promote the re-evaporation of MoO_2 by rapidly increasing the temperature of the molten zone. These authors have also grown $SrRuO_3$ (SRO), an archetypal perovskite ferromagnetic metal, which also presents the deposit of RuO_2 near the melting point. Thus, by applying 10 atmospheres of Ar with 10% O_2 at a growth rate of 7 mm/h from a raw material with a 0.05 at% excess of Ru, a stable crystal growth without fluctuations of the material rod or the molten zone was achieved. These two volatile materials were synthetized through LDFZ technique, in which the use of various lasers allows a uniform irradiation intensity distribution on the periphery of the raw material. In addition, a vertical irradiation intensity distribution can be designed to have flat-shape or bell-shape irradiations for relaxation of residual thermal strain in the grown crystal [22,32].

The LDFZ technique has been also recently applied to produce incongruent melting materials like the Y-type hexaferrite $Ba_2Co_2Fe_{12}O_{22}$ conventionally grown by a flux method [32]. So, single crystals of the multiferroic compound were successfully grown at 10 atmospheres and a slow growth rate of 1 mm/h from a seed crystal having the desired composition and crystal structure. Indeed, crystals of $BiFeO_3$ and $La_{2-x}Ba_xCuO_4$ were obtained [22], as was also mentioned in Section 2, avoiding the stability problems caused by the gentle temperature gradient when growing in conventional LFZ. However, conventional LFZ has allowed us to produce other incongruent melting materials through the years [192,193]. For example, Andreeta et al., in 1999 [193], were able to grow single-crystal fibers of the dielectric $SrHfO_3$ in air from green rods. Its properties were found to be influenced by incongruent melting since, depending on the growth rate, surface inclusions and compositional variations were observed. Some years after, $Tb_3Al_5O_{12}$ was also successfully produced in a modified LFZ setup, adapted with four halogen lamps to reduce thermal gradients, favoring TAG crystallization [30,31,118], as mentioned earlier in Section 4. Likewise, iron aluminate garnet ($Y_3Fe_5O_{12}$) is another incongruent melting material, which was easily grown in air using conventional LFZ by Sekijima et al., in 1999 [119], and by Lim et al., in 2000 [194]. It is useful for monitoring unique magneto-optical properties in the near infrared, making it suitable as an infrared isolator, optical switch, and spatial light modulator, as well as in other sensor applications. In the beginning of the 21st century, researchers grew through the LFZ or LHPG technique other examples of incongruent materials. For example, Chen et al., in 2002 [195], successfully grew metastable $BaTiO_3$ crystal fibers doped with calcium oxide, namely, $Ba_{1-x}Ca_xTiO_3$ (x = 0.1, 0.2). Taking advantage of their tetragonal structure, the growth from both $SrTiO_3$ and $Ba_{0.8}Ca_{0.1}TiO_3$ seeds was demonstrated. The growth of potassium lithium niobate (KLN) single crystal suitable for second harmonic generation with blue laser emission [86–88] may also be cited once more here, as an important example.

8. Future Perspectives

The Laser Floating Zone (LFZ) technique reviewed in this paper, also known as Laser-Heated Pedestal Growth (LHPG), could be considered as an ideal, environmentally benign

method to obtain high-quality single crystals within a very short time span, while minimizing the use of starting precursors and increasing overall energy efficiency with respect to other bulk-crystal growth methods. From these points of view, it is ideal to fulfill the long-sought desire to advance the understanding of fundamental physico-chemical phenomena at a fast pace. In essence, it complies perfectly with the message transmitted in a recent sentence by Schmehr et al., in 2019 [23]: "The availability of pristine single crystals is essential to the discovery of new physical phenomena in condensed matter physics". Perhaps the latter is a good indication that LFZ is essential toward the development of an important part of the future awaiting solid-state chemistry and physics, as well as materials science and the technological developments that follow from these.

Taking into account exclusively the growth of congruently melting materials in single-crystal cylinder or fiber form, LFZ provides, to a first approximation, important advantages regarding the use of small quantities of materials, crucible-free melt containment, and fast growth rates. The quality of the crystals obtained thus far has proven sufficient for their use in demonstrators and in high-technology devices. Crystals with good optical quality for laser resonators are a good example of their demonstrated use and future potential. For example, ultra-fast mode-locking lasers producing picosecond (10^{-12} s) and femtosecond (10^{-15} s) high-energy pulses at multi-GHz repetition rates [196] can be applied in a wide range of applications that include nonlinear optics, telecommunications, nanomachining, medical surgery, and environmental monitoring [197–200]. Likewise, this method is adequate to achieve high-quality crystals of small dimensions for compact and portable instruments, as discussed in Section 4. LFZ has enabled fabrication of high-quality photonic materials suitable to be used as optical isolators, amplifiers, or modulators, waveguides by embedding into adequate cylinders, scintillators, luminescent materials, temperature sensors, electro-optics, photorefractive materials, or selective emitters for silicon photovoltaic cells, among others.

More recent developments related to the use of different types of lasers, particularly diode lasers that may be deployed in various focusing configurations, have provided significant improvements on heating homogeneity and melt uniformity [32]. These affect not only the crystal quality, but potentially reduce the undesired appearance of microcracks, which make the crystal useless, or fail under further stress during use. In addition, these novel configurations enable the growth of incongruently melting phases, such as those considered in previous sections above, as well as phases that require particular atmosphere control. Examples of these include incongruently melting $Ba_2Co_2Fe_{12}O_{22}$, grown under O_2 atmosphere [32], and highly volatile $Nd_2Mo_2O_7$ and $SrRuO_3$, grown under Ar and Ar:O_2 atmospheres, respectively. An extreme case is the growth of the known volatile Li_2CuO_2 compound, achieved within a high-pressure (HP-LFZ) apparatus [23] and an 80:20 Ar:O_2 atmosphere. Thus, the demonstrated growth of non-congruent melting [26–29,82,83,114,188–192] or volatile [22,28,29,188] materials in a controlled, direct, and fast manner paves the way to explore the fabrication of crystal elements for already relevant, expected, and unforeseen applications in high technology.

Focusing on difficult-to-grow materials, we must highlight the recent work of Lai et al., in 2018, who studied how to design a nonlinear, hybrid, crystal-glass 3D metamaterial fiber with sub-wavelength fine structures [104]. They grew a large-scale harmonic crystal (Si^{4+}:γ-Al_2O_3) from a sapphire (α-Al_2O_3) crystal monolithically integrated into silica tubes. A hybrid crystal-glass metamaterial fiber was thus produced in a two-step process. Laser irradiation was followed by rapid cooling, to induce an inter-diffusion process where nucleation of large-sized harmonic crystals in anisotropic faceting was achieved. These open the possibility for attaining monolithically integrated dendrites for intracavity and resonant second harmonic generation (SHG) [104].

In the last decade, new, clean, and sustainable power-generation methods have been intensively investigated in attempts to control global warming. Innovative sustainable development is now accepted as a way of progress toward an improved environment, for which the design and development of novel materials able to be used in a plethora of

applications becomes an urgent necessity. In this sense, a breakthrough in the efficiency of thermoelectric (TE) materials will have an important technological and economic impact on the global energy balance. This may include novel approaches to develop advanced thermoelectric oxides, by in situ defects' engineering and nanostructuring, promoted by controlled redox reactions. These innovative aspects can be explored by LFZ processing under strongly non-equilibrium conditions for designing desired functional thermoelectric properties [29,122–124,137–145]. Moreover, the use of an externally applied current during the growth process (EALFZ) is a powerful tool to design and control microstructure, thus to improve transport properties. Particular attention needs to be given to the fabrication of prototypes based on LFZ-processed thermoelements, considering not only the present geometry achieved for the LFZ-obtained TE materials.

High-temperature superconducting ceramics have been among the most commonly studied materials with LFZ [29,122,125,133,160–162,164–182], probably because their anisotropic structure is ideal for directional solidification processing. As reviewed above, LFZ has demonstrated excellent microstructural transformations that result in high critical current elements in rod and tube geometries. These have been demonstrated to be competitive in several applications, particularly in superconducting current leads. These are used to connect electric power between room temperature and cryogenic temperatures, necessary for high-magnetic-field superconducting magnet operation, present for example in MRI machines, among other devices.

A most relevant advancement for superconductor processing is based on the EALFZ technique [29,122,127,128,134,186,187], which provides an additional control of texture, yields excellent results in terms of critical current values, and opens new frontiers to study the fundamental phenomena that stand behind controlled diffusion during directional solidification at large.

Future developments of LFZ within the superconductor materials domain should probably center at least around three aspects. First of all, on applying further and improving our understanding of electrically assisted phenomena during melting and solidification. Secondly, in exploring texturing of large-area, high-T_c coatings and films, which may find a number of attractive applications, including in attractive devices driven by levitation. Thirdly, modifying precursor, heating, and solidification geometries in order to improve the scalability of the method for industrial production.

A least explored aspect of LFZ entails the possibility of producing organic complex molecules in the form of crystalline fibers [120,121]. As suggested by the results reviewed above, a wide range of opportunities to explore bio-compatible applications may be envisioned. In addition, the production on geometries suitable to be employed, for example, in photonic devices, highly reduces the engineering, mechanical, and economical cost associated when an organic-based compound must be integrated into a commercial photonic device. These types of materials need intensive studies in order to establish a proper knowledge base for LFZ-processed organic compounds, and future efforts will determine the potential of the technique to address the intrinsic scientific and technical problems involved, particularly with respect to competing fabrication methods.

Finally, a universal advantage that may always be considered for the future evolution of LFZ is, as commented earlier, its facile, low cost, and turnaround productivity of an ample collection of materials in single-crystal form and with convenient size for physical property characterization and demonstration prototypes. These would apply to wide-open disciplines of science and technology. The technique may gain relevance if consideration is given to miniaturization of apparatus and the achievement of higher mechanical precision. Together with air-cooled, small-size, and high-beam-quality lasers recently available at lower cost and high durability, LFZ may end up being incorporated into many laboratories worldwide for quick turnaround and convenient materials' processing exploration purposes. It will certainly contribute to the advancement of both fundamental understanding of physical phenomena and developments of new devices.

Funding: G.F.d.l.F. and L.A.A. acknowledge support from Gobierno de Aragón "Construyendo Europa desde Aragón (research group T54_20R). This work was also developed within the scope of the projects, i3N, UIDB/50025/2020 and UIDP/50025/2020, financed by national funds through the FCT/MCTES.

Acknowledgments: F.R.-G. acknowledges Aleixo, Xabier, and Diana for their comprehension despite reducing our time together.

Conflicts of Interest: The authors declare no conflict of interest.

References

1. García-Ruiz, J.M.; Otálora, F. *Crystal Growth in Geology: Patterns on the Rocks*, 2nd ed.; Elsevier B.V.: Amsterdam, The Netherlands, 2015; Volume 2.
2. Yang, G.; Park, S.J. Conventional and microwave hydrothermal synthesis and application of functional materials: A review. *Materials* **2019**, *12*, 1177. [CrossRef] [PubMed]
3. Pamplin, B.R. Introduction to Crystal Growth Methods. In *Crystal Growth*; Pamplin, B.R., Ed.; Pergamon Press Ltd.: Oxford, UK, 1980; pp. 1–21.
4. Friedrich, J. Methods for bulk growthof inorganic crystals: Crystal growth. In *Reference Module in Materials Science and Materials Engineering*; Elsevier Ltd.: Amsterdam, The Netherlands, 2016; pp. 1–16.
5. Alshourbagy, M. Development of Single Crystal Fibers for Optical, Scintillation and Mechanical Applications. Ph.D. Thesis, Università di Pisa, Pisa, Italy, 2005.
6. Haggerty, J.S. *Production of Fibers by a Floating Zone Fiber Drawing Technique*; Final Report NASA-CR-120948; National Aeronautics and Space Administration NASA: Washington, DC, USA, 1972.
7. Feigelson, R.S. Pulling optical fibers. *J. Cryst. Growth* **1986**, *79*, 669–680. [CrossRef]
8. Rudolph, P.; Fukuda, T. Fiber crystal growth from the melt. *Cryst. Res. Technol.* **1999**, *34*, 3–40. [CrossRef]
9. Andreeta, M.R.B.; Hernandes, A.C. Chapter 13: Laser-heated pedestal growth of oxide fibers. In *Springer Handbook of Crystal Growth*; Dhanaraj, G., Byrappa, K., Prasad, V., Dudley, M., Eds.; Springer: Berlin, Germany, 2010; pp. 393–432.
10. Revcolevschi, A. Application of a treating method based on concentration of radiant energy to X-rays diffraction until 3000 °C and to high temperature crystal growth. *Rev. Int. Hautes Temp.* **1970**, *7*, 73–94.
11. Dhalenne, G.; Revcolevschi, A.; Collongues, R. Application de la methode de zone flottante a la croissance de bicristaux d'oxydes refractaires. *Mater. Res. Bull.* **1972**, *7*, 933–941. [CrossRef]
12. Revcolevschi, A.; Jegoudez, J. Growth of large high-Tc single crystals by the floating zone method: A review. *Prog. Mater. Sci.* **1997**, *42*, 321–339. [CrossRef]
13. Koohpayeh, S.M.; Fort, D.; Abell, J.S. The optical floating zone technique: A review of experimental procedures with special reference to oxides. *Prog. Cryst. Growth Charact. Mater.* **2008**, *54*, 121–137. [CrossRef]
14. Dabkowska, H.A.; Dabkowski, A.B. Chapter 12. Crystal growth of oxides by optical floating zone technique. In *Springer Handbook of Crystal Growth*; Dhanaraj, G., Byrappa, K., Prasad, V., Dudley, M., Eds.; Springer: Berlin, Germany, 2010; pp. 367–391.
15. Phelan, W.A.; Zahn, J.; Kennedy, Z.; McQueen, T.M. Pushing boundaries: High pressure, supercritical optical floating zone materials discovery. *J. Solid State Chem.* **2019**, *270*, 705–709. [CrossRef]
16. Liu, F.; Goodman, B.A.; Tan, X.; Wang, X.; Chen, D.; Deng, W. Luminescence and EPR properties of high quality ruby crystals prepared by the optical floating zone method. *Opt. Mater.* **2019**, *91*, 183–188. [CrossRef]
17. Haihang, Y.; Changjiang, L.; Zhikun, Z.; Shimin, H.; Yunling, Y.; Rihua, M.; He, F.; Jingtai, Z. Single crystal growth and luminescence properties of YSH:Eu scintillator by optical floating zone method. *Chem. Phys Lett.* **2020**, *738*, 136916.
18. Xin, C.; Veber, P.; Guennou, M.; Toulouse, C.; Valle, N.; Hatnean, M.C.; Balakrishnan, G.; Haumont, R.; Saint-Martin, R.; Velasquez, M.; et al. Single crystal growth of $BaZrO_3$ from the melt at 2700 °C using optical floating zone technique and growth prospects from BaB_2O_4 flux at 1350 °C. *CrystEngComm* **2019**, *21*, 502–512. [CrossRef]
19. Wang, B.X.; Zheng, H.; Ren, Y.; Korgstad, M.; Mitchell, J.F.; Phelan, D. Single crystal growth of relaxor ferroelectric $Ba_2PrFeNb_4O_{15}$ by the optical floating zone method. *Cryst. Growth Des.* **2019**, *19*, 7249–7256. [CrossRef]
20. Hatnean, M.C.; Petrenko, O.A.; Lees, M.R.; Orton, T.E.; Balakrishnan, G. Optical floating zone crystal growth of rare-earth disilicates, $R_2Si_2O_7$ (R = Er, Ho, and Tm). *Cryst. Growth Des.* **2020**, *20*, 6636–6648. [CrossRef]
21. Rey-García, F.; Bao-Varela, C.; Costa, F.M. Laser floating zone: General overview focusing on the oxyorthosilicates growth. In *Synthesis Methods and Crystallization*; Marzouki, R., Ed.; Intechopen: London, UK, 2019.
22. Ito, T.; Ushiyama, T.; Yanagisawa, Y.; Tomioka, Y.; Shindo, I.; Yanase, A. Laser-diode-heated floating zone (LDFZ) method appropriate to crystal growth of incongruently melting materials. *J. Cryst. Growth* **2013**, *363*, 264–269. [CrossRef]
23. Schmehr, J.L.; Aling, M.; Zoghlin, E.; Wilson, S.D. High-pressure laser floating zone furnace. *arXiv* **2019**, arXiv:1902.05937v1. [CrossRef] [PubMed]
24. Fejer, M.M.; Byer, R.L.; Feigelson, R.S.; Kway, W. Growth and characterization of single crystal refractory oxide fibers. In *Advances in Infrared Fibers II; Proceedings of the 2nd Meeting, Los Angeles, CA, USA, 26–28 August 2004*; SPIE: Bellingham, WA, USA, 1982; p. A83-4662122-74.

25. Fejer, M.M.; Nightingale, J.L.; Magel, G.A.; Byer, R.L. Laser-Heated miniature pedestal growth apparatus for single-crystal optical fibers. *Rev. Sci. Instrum.* **1984**, *55*, 1791–1796. [CrossRef]
26. Martin, C.W. Reflecting Optical Objective System. U.S. Patent 2457253, 28 December 1948.
27. Nubling, R.K.; Harrington, J.A. Optical properties of single-crystal sapphire fibers. *Appl. Opt.* **1997**, *36*, 5934–5940. [CrossRef]
28. Bruek, E.; Gelders, H.J.; Harrison, B.J.; Menovsky, A.A. Laser-heated fibre pedestal growth under UHV conditions. *J. Cryst. Growth* **1996**, *166*, 394–397. [CrossRef]
29. Carrasco, M.F.; Silva, R.F.; Vieira, J.M.; Costa, F.M. Electrical field freezing effect on laser floating zone (LFZ)-grown $Bi_2Sr_2Cu_4O_{11}$ superconducting fibres. *Supercond. Sci. Technol.* **2004**, *17*, 612–619. [CrossRef]
30. Geho, M.; Sekijima, T.; Fujii, T. Growth of terbium aluminum garnet ($Tb_3Al_5O_{12}$; TAG) single crystals by the hybrid laser floating zone machine. *J. Cryst. Growth* **2004**, *267*, 188–193. [CrossRef]
31. Sekijima, T.; Geho, M. Method for manufacturing terbium aluminium-based paramagnetic garnet single crystal. European Patent No. EP1391544A2, 25 February 2004.
32. Kaneko, Y.; Tokura, Y. Floating zone surface equipped with a high power laser of 1 kW composed of five smart beams. *J. Cryst. Growth* **2020**, *533*, 125435. [CrossRef]
33. Crystal System Corporation. Available online: http://www.crystalsys.co.jp/english/product04_e.html (accessed on 18 September 2020).
34. Quantum Design International. Available online: https://qd-europe.com/at/en/product/1-kw-and-2-kw-laser-furnace-for-the-production-of-long-single-crystals/ (accessed on 18 September 2020).
35. Wang, W.L.; Wang, J.S.; Huang, Y.C.; Liu, L.W.; Huang, S.L.; Cheng, W.H. Few-mode Cr-doped crystalline core fibers for fiber amplifier. *IEEE Photon. Technol. Lett.* **2012**, *24*, 1628–1631. [CrossRef]
36. Kim, W.; Florea, C.; Gibson, D.; Peele, J.; Askins, C.; Shaw, B.; Bowman, S.; O'Connor, S.; Bayya, S.; Aggarwal, I.; et al. Crystal fibers for high power lasers. In *Fiber Lasers X: Technology, Systems and Applications, Proceedings of the SPIE LASE, San Francisco, CA, USA, 2–7 February 2013*; Hendow, S.T., Ed.; SPIE: Bellingham, WA, USA, 2013; Volume 8601, p. 86012Z.
37. Nie, C.D.; Bera, S.; Melzer, J.E.; Harrington, J.A.; Dreyer, E.F.C.; Rand, S.C.; Trembath-Reichert, S.; Hoef, C.D. Erbium distribution in single crystal YAG fibers grown by laser-heated pedestal growth technique. In *Solid State Lasers XXIV: Technology and Devices, Proceedings of the SPIE LASE, San Francisco, CA, USA, 8–10 February 2015*; Clarkson, W.A., Shori, R.K., Eds.; SPIE: Bellingham, WA, USA, 2015; Volume 9342, p. 934204.
38. Bera, S.; Ohodnicki, P., Jr.; Collins, K.; Fortner, M.; Picard, Y.N.; Liu, B.; Buric, M. Dopant segregation in YAG single crystal fibers grown by the laser heated pedestal growth technique. *J. Cryst. Growth* **2020**, *547*, 125801. [CrossRef]
39. Lai, C.C.; Lo, C.Y.; Hsieh, T.H.; Tsai, W.S.; Nguyen, D.H.; Ma, Y.R. Ligand-driven and full-color-tunable fiber source: Toward next-generation clinic fiber-endoscope tomography with cellular resolution. *ACS Omega* **2016**, *1*, 552–565. [CrossRef] [PubMed]
40. Zhu, X.S.; Harrington, J.A.; Lautsen, B.T.; DeShazer, L.G. Single-crystal YAG fiber optics for the transmission of high energy laser energy. In *Optical Fibers, Sensors, and Devices for Biomedical Diagnostics and Treatment XI, Proceeding of SPIE BIOS, San Francisco, CA, USA*, 22 January 2011; Gannot, I., Ed.; SPIE: Bellingham, WA, USA, 2011; Volume 7894, p. 789415.
41. Lautsen, B.T.; Harrington, J.A. Fabrication and optical properties of single-crystal YAG fiber optics. In *Solid State Lasers XXI: Technology and Devices, Proceedings of the SPIE LASE, San Francisco, United States, 2012*; Clarkson, W.A., Shori, R.K., Eds.; International Society for Optics and Photonics: Bellingham, WA, USA, 2012; Volume 8235, p. 823505.
42. Harrington, J.A. Single-crystal fiber optics: A review. In *Solid State Lasers XXIII: Technology and Devices, Proceedings of the SPIE LASE, San Francisco, CA, USA, 21–26 January 2014*; Clarkson, W.A., Shori, R.K., Eds.; SPIE: Bellingham, WA, USA, 2014; Volume 8959, p. 895901.
43. Pastor, J.Y.; Llorca, J.; Salazar, A.; Oliete, P.; de Francisco, I.; Peña, J.I. Mechanical properties of melt-grown alumina-yttrium aluminum garnet eutectics up to 1900K. *J. Am. Ceram. Soc.* **2005**, *88*, 1488–1495. [CrossRef]
44. The Library of Manufacturing. Available online: https://thelibraryofmanufacturing.com/alt_powder_processes.html (accessed on 18 September 2020).
45. Rudolph, P.; Kakimoto, K. Crystal growth from the melt under external force fields. *MRS Bull.* **2009**, *34*, 252–258. [CrossRef]
46. Stone, J.; Burrus, C.A.; Dentai, A.G.; Miller, B.I. Nd:YAG single-crystal fiber laser: Room-tempearature cw operation using a single LED as an end pump. *Appl. Phys. Lett.* **1976**, *29*, 37–39. [CrossRef]
47. RP Photonics. Available online: https://www.rp-photonics.com/laser_crystals.html?s=ak (accessed on 26 September 2020).
48. Rey-García, F.; Costa, F.M.; Zaldo, C. Laser floating zone growth of Yb, or Nd, doped $(Lu_{0.3}Gd_{0.7})_2SiO_5$ oxyorthosilicate single-crystal rods with efficient laser performance. *J. Mater. Chem. C* **2020**, *8*, 2065–2073. [CrossRef]
49. Maxwell, G.; Ponting, B.; Gebremichel, E.; Magana, R. Advances in single-crystal fibers and thin rods grown by laser heated pedestal growth. *Crystals* **2017**, *7*, 12. [CrossRef]
50. Kim, W.; Shaw, B.; Bayya, S.; Askins, C.; Peele, J.; Rhonehouse, D.; Meyers, J.; Thapa, R.; Gibson, D.; Sanghera, J. Cladded single crystal fibers for high power fiber lasers. In *Photonic Fiber and Crystal Devices: Advances in Materials and Innovations in Device Applications X, Proceedings of the SPIE Optical Engineering + Applications, San Diego, CA, USA, 28–29 August 2016*; Yin, S., Guo, R., Eds.; SPIE: Bellingham, WA, USA, 2016; Volume 9958, p. 99580O.
51. Wang, T.; Zhang, J.; Zhang, N.; Wang, S.; Wu, B.; Jia, Z.; Tao, X. The characteristics of high-quality Yb:YAG single crystal fibers grown by a LHPG method and the effects of their discoloration. *RSC Adv.* **2019**, *9*, 22567–22575. [CrossRef]
52. Rey-García, F.; Rodrigues, J.; Monteiro, T.; Costa, F.M. Intense red emission on dilute Mn-doped CaYAlO4-based ceramics obtained by laser floating zone. *J. Mater. Sci. Mater. Electron.* **2019**, *30*, 21454–21464. [CrossRef]

53. Ishibashi, S.; Naganuma, K. Diode-pumped Cr^{4+}:YAG single-crystal fiber laser. In *Advanced Solid State Lasers*; OSA Technical Digest Series, Paper MD4; Optical Society of America: Washington, DC, USA, 2000.
54. Shen, Y.; Chen, S.; Zhao, W.; Chen, J. Composite Cr^{4+}:YAG—Nd^{3+}:YAG crystal fiber: Growth characteristics and passively Q-switched laser operation. In *Materials, Devices, and Systems for Display and Lighting, Proceedings of the Photonics Asia, Shanghai, China, 14–18 October 2002*; Gan, F., Wu, M.H., Kimerling, L.C., Eds.; SPIE: Bellingham, WA, USA, 2002; Volume 4918, pp. 20–27.
55. Boulon, G. Yb^{3+}-doped oxide crystals for diode-pumped solid state lasers: Crystal growth, optical spectroscopy, new criteria of evaluation and combinatorial approach. *Opt. Mater.* **2003**, *22*, 85–87. [CrossRef]
56. Yoshikawa, A.; Boulon, G.; Laversenne, L.; Canibano, H.; Lebbou, K. Growth and spectroscopic analysis of Yb^{3+}-doped $Y_3Al_5O_{12}$ fiber single crystals. *J. Appl. Phys.* **2003**, *94*, 5479. [CrossRef]
57. Ye, L.; Qiu, Y.; He, J.; Shen, Y.; He, S. Growth and fluorescence characteristics of Cr^{3+}:YAG crystal fiber for temperature sensor from −10 °C to 500 °C. In *Advanced Materials and Devices for Sensing and Imaging II, Proceedings of the Photonics Asia, Beijing, China, 8–11 November 2004*; Wang, A., Zhang, Y., Ishii, Y., Eds.; SPIE: Bellingham, WA, USA, 2005; Volume 5633, pp. 177–184.
58. Bufetova, G.A.; Kashin, V.V.; Nikolaev, D.A.; Rusanov, S.Y.; Seregin, V.F.; Tsvetkov, V.B.; Shcherbakov, I.A.; Yakovlev, A.A. Neodymium-doped graded-index single-crystal fibre lasers. *Kvantovaya Elektron.* **2006**, *36*, 616–619. [CrossRef]
59. Chen, P.Y.; Chang, C.L.; Lan, C.W.; Cheng, W.H.; Huang, S.L. Two-Dimensional simulations on heat transfer and fluid flow for yttrium aluminium garnet single-crystal fiber in laser-heated pedestal growth system. *Jpn. J. Appl. Phys.* **2009**, *48*, 115504. [CrossRef]
60. Lai, C.C.; Lin, Y.S.; Huang, K.Y.; Huang, S.L. Effect of nanocrystal structures on interface of Cr-doped yttrium aluminium garnet double-clad crystal fiber. *Jpn. J. Appl. Phys.* **2009**, *48*, 122502. [CrossRef]
61. Yi, J.Y.; Huang, K.Y.; Lai, C.C.; Peng, H.; Chen, L.H.; Huang, S.L. Ytterbium-Doped yettrium aluminum garnet crystal fiber multipass ring laser. *Jpn. J. Appl. Phys.* **2010**, *49*, 122701. [CrossRef]
62. Chang, C.L.; Huang, S.L.; Lo, C.Y.; Huang, K.Y.; Lan, C.W.; Cheng, W.H.; Chen, P.Y. Simulation and experiment on laser-heated pedestal growth of chromium-doped yttrium aluminum garnet single-crystal fiber. *J. Cryst. Growth* **2011**, *318*, 674–678. [CrossRef]
63. Kim, W.; Florea, C.; Baker, C.; Gibson, D.; Shaw, L.B.; Bowman, S.; O'Connor, S.; Villalobos, G.; Bayya, S.; Aggarwal, I.D.; et al. Single crystal fibers for high power lasers. In *High-Power Lasers 2012: Technology and Systems, Proceedings of the SPIE Security + Defence, Edinburgh, UK, 24–26 September 2012*; Ackermann, H., Bohn, W.L., Eds.; SPIE: Bellingham, WA, USA, 2012; Volume 8547, p. 85470K.
64. Hsu, K.Y.; Yang, M.H.; Jheng, D.Y.; Lai, C.C.; Huang, S.L.; Mennemann, K.; Dietrich, V. Cladding YAG crystal fibers with high-index glasses for reducing the number of guided modes. *Opt. Mater. Express* **2013**, *3*, 813–820. [CrossRef]
65. Hsu, K.Y.; Yang, M.H.; Jheng, D.Y.; Mennemann, K.; Dietrich, V.; Dubinskii, M. Single crystalline YAG-core fiber with a lanthanum dense flint glass cladding. In Proceedings of the Conference on Lasers and Electro-optics Pacific Rim (CLEO-PR, 2013), Kyoto, Japan, 30 June–4 July 2013. paper ThA2-5.
66. Lai, C.C.; Huang, S.L.; Wang, S.H.; Ho, W.C.; Liu, S.K.; Tsai, C.N. Strongly enhancing Cr^{4+} broadband emissions in strained crystalline core of Cr:YAG double-clad fiber amplifier. In Proceedings of the Conference on Lasers and Electro-optics Pacific Rim (CLEO-PR, 2013), Kyoto, Japan, 30 June–4 July 2013. paper ThA1-5.
67. Maxwell, G.; Soleimani, N.; Ponting, B.; Gebremichael, E. Coilable single crystals fibers of doped-YAG for high power laser applications. In *Laser Technology for Defense and Security IX, Proceedings of the SPIE Defense, Security, and Sensing, Baltimore, MD, USA, 29 April–3 May 2013*; Dubinskii, M., Post, S.G., Eds.; SPIE: Bellingham, WA, USA, 2013; Volume 8733, p. 87330T.
68. Wang, W.L.; Tseng, Y.H.; Cheng, W.H.; Wang, J.S. Silica cladded Nd^{3+}:YAG single crystal core optical fiber and its submicron residual stress detection. *Opt. Mater. Express* **2014**, *4*, 656–661. [CrossRef]
69. Oliete, P.B.; Mesa, M.C.; Merino, R.I.; Orera, V.M. Directionally solidified Al_2O_3-$Yb_3Al_5O_{12}$ eutectics for selective emitters. *Sol. Energy Mater. Sol. Cells* **2016**, *144*, 405–410. [CrossRef]
70. Liu, C.N.; Wang, T.H.; Rou, T.S.; Chen, N.K.; Huang, S.L.; Cheng, W.H. Higher gain of single-mode Cr-doped fibers employing optimized molten-zone growth. *J. Light. Technol.* **2017**, *35*, 4930–4936. [CrossRef]
71. Bufetova, G.A.; Rusanov, S.Y.; Seregin, V.F.; Pyrkov, Y.N.; Tsvetkov, V.B. Dynamics of Er^{3+}:YAG thermal radiation spectra near solid-melt interface at single crystal fiber growth process. *J. Cryst. Growth* **2019**, *506*, 165–170. [CrossRef]
72. Kim, W.; Bayya, S.; Shaw, B.; Myers, J.; Qadri, S.N.; Thapa, R.; Gibson, D.; McClain, C.; Kung, F.; Kolis, J.; et al. Hydrothermally cladded crystalline fibers for laser applications. *Opt. Mater. Express* **2019**, *9*, 2716–2728. [CrossRef]
73. Bao, R.; An, N.; Ye, L.; Wang, L.G. Wide-range temperature sensor based on enhanced up-conversion luminescence in Er^{3+}/Yb^{3+} co-doped Y_2O_3 crystal fiber. *Opt. Fiber Technol.* **2019**, *52*, 101989. [CrossRef]
74. An, N.; Ye, L.; Bao, R.; Yue, L.; Wang, L.G. Up-Conversion luminescence characteristics and temperature sensing of Y_2O_3:Ho^{3+}/Yb^{3+} single crystal fiber. *J. Lumin.* **2019**, *215*, 116657. [CrossRef]
75. Romero, J.J.; Montoya, E.; Bausá, L.E.; Agulló-Rueda, F.; Andreeta, M.R.B.; Hernandes, A.C. Multiwavelength laser action of Nd^{3+}:$YAlO_3$ single crystals grown by the laser heated pedestal growth method. *Opt. Mater.* **2004**, *24*, 643–650. [CrossRef]
76. Rey-García, F.; Ben Sedrine, N.; Soares, M.R.; Fernandes, A.J.S.; Lopes, A.B.; Ferreira, N.M.; Monteiro, T.; Costa, F.M. Structural and optical characterization of Gd_2SiO_5 crystalline fibres obtained by laser floating zone. *Opt. Mater. Express* **2017**, *7*, 868–879. [CrossRef]
77. Rey-García, F.; Rodrigues, J.; Fernandes, A.J.S.; Soares, M.R.; Monteiro, T.; Costa, F.M. $(Lu_{0.3}Gd_{0.7})_2SiO_5$:$Y^{3+}$ single crystals grown by the laser floating zone method: Structural and optical studies. *CrystEngComm.* **2018**, *20*, 7386–7394. [CrossRef]

78. Rey-García, F.; Fernandes, A.J.S.; Costa, F.M. Influence of Lu content on $(Lu_xGd_{1-x})_2SiO_5$ oxyorthosilicates grown by Laser Floating Zone: Structural studies and transparency. *Mater. Res. Bull.* **2019**, *112*, 413–419. [CrossRef]
79. Andreeta, M.R.B.; de Camargo, A.S.S.; Nunes, L.A.O.; Hernandes, A.C. Transparent and inclusion-free $RE_{1-x}La_xVO_4$ (RE = Gd, Y) single crystal fibers grown by LHPG technique. *J. Cryst. Growth* **2006**, *291*, 117–122. [CrossRef]
80. De Camargo, A.S.S.; Ferrari, C.R.; Silva, R.A.; Nunes, L.A.O.; Hernandes, A.C.; Andreeta, J.P. Spectroscopic features of erbium-doped CaM_2O_6 (M = Nb, Ta) single crystal fibers grown by the laser-heated pedestal growth technique. *J. Lumin.* **2008**, *128*, 223–226. [CrossRef]
81. Almeida, R.M.; Matinaga, F.M.; Andreeta, M.R.B.; Hernandes, A.C.; Dias, A.; Moreira, R.L. Polymorphic-induced transformations in $CaTa_2O_6$ single-crystal fibers obtained by laser-heated pedestal growth. *Cryst. Growth Des.* **2013**, *13*, 5289–5294. [CrossRef]
82. Reyes-Ardila, D.; Barbosa, L.B.; Andreeta, J.P. Bifocal spherical mirror for laser processing. *Rev. Sci. Instrum.* **2001**, *72*, 4415. [CrossRef]
83. Andreeta, M.R.B.; Caraschi, L.C.; Hernandes, A.C. Automatic diameter control system applied to the laser heated pedestal growth technique. *Mater. Res.* **2002**, *6*, 107–110. [CrossRef]
84. Chen, C.Y.; Chen, J.C.; Lai, Y.J. Investigations of the growth mechanism of stoichiometric $LiNbO_3$ fibers grown by the laser-heated pedestal growth method. *J. Cryst. Growth* **2005**, *275*, e763–e768. [CrossRef]
85. Chen, C.Y.; Chen, J.C.; Chia, C.T. Growth and optical properties of different compositions of $LiNbO_3$ single crystal fibers. *Opt. Mater.* **2007**, *30*, 393–398. [CrossRef]
86. Matsukura, M.; Takeyama, T.; Karaki, T.; Adachi, M. Domain structures in $K_3Li_{2-x}Nb_{5+x}O_{15+2x}$ single-crystal fibers produced by the laser-heated pedestal growth technique. *Jpn. J. Appl. Phys.* **2001**, *40*, 5783. [CrossRef]
87. Guo, Y.J.; Xu, Y.H.; Yang, C.H. Influence of Zn doping on the optical properties of KLN single crystal. *J. Mater. Sci.* **2004**, *39*, 4027–4029. [CrossRef]
88. Maxwell, G.; Dalton, D.; Petersen, A.B. Second harmonic generation below 400 nm using potassium lithium niobate from laser-heated pedestal growth. In *Advances in Optical Materials*; OSA Technical Digest (CD), Paper AIThE4; Optical Society of America: Washington, DC, USA, 2011.
89. Bourson, P.; Aillerie, M.; Cochez, M.; Ferriol, M.; Zhang, Y.; Guilbert, L. Characterization of iron substitution process in Fe:$LiNbO_3$ single crystal fibers by polaron measurements. *Opt. Mater.* **2003**, *24*, 111–116. [CrossRef]
90. Cochez, M.; Ferriol, M.; Bourson, P.; Aillerie, M. Influence of the dopant concentration on the OH- absorption band in Fe-doped $LiNbO_3$ single-crystal fibers. *Opt. Mater.* **2003**, *21*, 775–781. [CrossRef]
91. Nagashio, K.; Watcharapasorn, A.; DeMattei, R.C.; Feigelson, R.S. Fiber growth of near-stoichiometric $LiNbO_3$ single crystals by the laser-heated pedestal growth method. *J. Cryst. Growth* **2004**, *265*, 190–197. [CrossRef]
92. Lee, L.M.; Kuo, C.C.; Chen, J.C.; Chou, T.S.; Cho, Y.C.; Huang, S.L.; Lee, H.W. Periodical poling of MgO doped lithium niobate crystal fiber by modulated pyroelectric field. *Opt. Commun.* **2005**, *253*, 375–381. [CrossRef]
93. Kashin, V.V.; Nikolaev, D.A.; Rusanov, S.Y.; Tsvetkov, V.B. Laser radiation frequency doubling in a single-crystal fibre based on a stoichiometric $LiNbO_3$ crystal. *Quantum Electron.* **2015**, *45*, 47–49. [CrossRef]
94. Graça, M.P.F.; Peixoto, M.V.; Ferreira, N.; Rodrigues, J.; Nico, C.; Costa, F.M.; Monteiro, T. Optical and dielectric behaviour of $EuNbO_4$ crystals. *J. Mater. Chem. C* **2013**, *1*, 2913–2919. [CrossRef]
95. Santos, N.F.; Rodrigues, J.; Fernandes, A.J.S.; Alves, L.C.; Alves, E.; Costa, F.M.; Monteiro, T. Optical properties of LFZ grown β-Ga_2O_3:Eu^{3+} fibres. *Appl. Surf. Sci.* **2012**, *258*, 9157–9161. [CrossRef]
96. Seat, H.C. Growth and Characterization of Single-Crystal Fibres for SENSING applications. Ph.D. Thesis, University of Glasgow, Glasgow, UK, 2001.
97. Seat, H.C.; Sharp, J.H. Er^{3+} + Yb^{3+}-codoped Al_2O_3 crystal fibers for high-temperature sensing. *Meas. Sci. Technol.* **2003**, *14*, 279–285. [CrossRef]
98. Liu, C.M.; Chen, J.C.; Chiang, C.H.; Hu, L.J.; Lin, S.P. Mg-doped sapphire crystal fibers grown by laser-heated pedestal growth method. *Jpn. J. Appl. Phys.* **2006**, *45*, 194–199. [CrossRef]
99. Rodrigues, J.; Peres, M.; Fernandes, A.J.S.; Graça, M.P.F.; Sobolev, N.A.; Costa, F.M.; Monteiro, T. Structural, optical and magnetic resonance properties of TiO_2 fibre grown by laser floating zone technique. *Appl. Surf. Sci.* **2012**, *258*, 9143–9147. [CrossRef]
100. Bufetova, G.A.; Rusanov, S.Y.; Seregin, V.F.; Pyrkov, Y.N.; Tsvetkov, V.B. Temperature and emissivity measurements at the sapphire single crystal fiber growth process. *J. Cryst. Growth* **2017**, *480*, 85–89. [CrossRef]
101. Liu, B.; Yu, Y.; Bera, S.; Buric, M.; Chorpening, B.; Ohodnicki, P. Study of the molten zone profile and defect formation during laser heated pedestal growth. In *Micro- and Nanotechnology Sensors, Systems, and Applications XI, Proceedings of the SPIE Defense + Commercial Sensing, Baltimore, MD, USA, 14–18 April 2019*; George, T., Saif Islam, M., Eds.; SPIE: Bellingham, WA, USA, 2019; Volume 10982, p. 109822K.
102. Dragic, P.; Hawkins, T.; Foy, P.; Morris, S.; Ballato, J. Sapphire-derived all-glass optical fibres. *Nat. Photonics* **2012**, *6*, 627–633. [CrossRef]
103. Lai, C.C.; Gao, W.T.; Nguyen, D.H.; Ma, Y.R.; Cheng, N.C.; Wang, S.C.; Tjiu, J.W.; Huang, C.M. Toward single-mode active crystal fibers for next-generation high-power fiber devices. *ACS Appl. Mater. Interfaces* **2014**, *6*, 13928–13936. [CrossRef] [PubMed]
104. Lai, C.C.; Lo, C.Y.; Huang, J.Z.; Fang Chiang, C.C.; Nguyen, D.H.; Chen, Y.P.; Liao, C.D. Architecting a nonlinear hybrid crystal-glass metamaterial fiber for all-optical photonic integration. *J. Mater. Chem. C* **2018**, *6*, 1659–1669. [CrossRef]
105. FindLight Blog. Available online: https://www.findlight.net/blog/2017/06/17/laser-crystals/ (accessed on 26 September 2020).

106. Laversenne, L.; Guyot, Y.; Goutaudier, C.; Cohen-Adad, M.T.; Boulon, G. Optimization of spectroscopic properties of Yb^{3+}-doped refractory sesquioxides: Cubic Y_2O_3, Lu_2O3 and monoclinic Gd_2O_3. *Opt. Mater.* **2001**, *16*, 475–483. [CrossRef]
107. Laversenne, L.; Goutaudier, C.; Guyot, Y.; Cohen-Adad, M.T.; Boulon, G. Growth of rare earth (RE) doped concentration gradient crystal fibers and analysis of dynamical processes of laser resonant transitions in RE-doped Y_2O_3 (RE = Yb^{3+}, Er^{3+}, Ho^{3+}). *J. Alloys Compd.* **2002**, *341*, 214–219. [CrossRef]
108. Saggioro, B.Z.; Andreeta, M.R.B.; Hernandes, A.C.; Macatrão, M.; Peres, M.; Costa, F.M.; Monteiro, T.; Franco, N.; Alves, E. Effect of Eu_2O_3 doing on Ta_2O_5 crystal growth by the laser-heated pedestal technique. *J. Cryst. Growth* **2010**, *313*, 62–67. [CrossRef]
109. Boulon, G.; Ito, M.; Goutaudier, C.; Guyot, Y. Advances in growth of fiber crystal by the LHPG technique. Application to the optimization of Yb^{3+}-doped CaF_2 laser crystals. *J. Cryst. Growth* **2006**, *292*, 230–235. [CrossRef]
110. Boulon, G.; Guyot, Y.; Yoshikawa, A. Optimization of the gain in Yb^{3+}-doped cubic laser crystals of 99.99% purity. *J. Rare Earth* **2009**, *27*, 616–618. [CrossRef]
111. Carvalho, R.G.; Fernandes, A.J.S.; Oliveira, F.J.; Alves, E.; Franco, N.; Louro, C.; Silva, R.F.; Costa, F.M. Single and polycrystalline mullite fibres grown by laser floating zone technique. *J. Eur. Ceram. Soc.* **2010**, *30*, 3311–3318. [CrossRef]
112. Rey-García, F.; Ben Sedrine, N.; Fernandes, A.J.S.; Monteiro, T.; Costa, F.M. Shifting Lu_2SiO_5 crystal to eutectic structure by laser floating zone. *J. Eur. Ceram. Soc.* **2018**, *38*, 2059–2067. [CrossRef]
113. Soares, M.R.N.; Ferro, M.; Costa, F.M.; Monteiro, T. Upconversion luminescence and blackbody radiation in tetragonal YSZ co-doped with Tm^{3+} and Yb^{3+}. *Nanoscale* **2015**, *7*, 19958–19969. [CrossRef] [PubMed]
114. Philippen, J.; Guguschev, C.; Klimm, D. Single crystal fiber growth of cerium doped strontium yttrate, SrY_2O_4:Ce^{3+}. *J. Cryst. Growth* **2017**, *459*, 17–22. [CrossRef]
115. Rueda, J.E.; Hernandes, A.C. Técnica rápida de producción de monocristales de titanato de estroncio con fotoconductividad persistente. *Rev. Infometr. Ser. Ing. Básicas Agríc.* **2020**, *3*, 8–16.
116. Ren, Q.; Su, H.; Zhang, J.; Ma, W.; Cao, Y.; Chen, J.; Liu, L.; Fu, H. Directional solidification and growth characteristics of $Al_2O_3/Er_3Al_5O_{12}/ZrO_2$ ternary eutectic ceramic by laser floating zone melting. *J. Mater. Sci.* **2017**, *52*, 5559–5568. [CrossRef]
117. Mesa, M.C.; Oliete, P.B.; Larrea, A.; Orera, V.M. Directionally solidified Al_2O_3-$Er_3Al_5O_{12}$-ZrO_2 eutectic ceramics with interpenetrating or nanofibrillar microstructure: Residual stress analysis. *J. Am. Ceram. Soc.* **2012**, *95*, 1138–1146. [CrossRef]
118. Geho, M.; Sekijima, T.; Fujii, T. Growth mechanism of incongruently melting terbium aluminum garnet ($Tb_3Al_5O_{12}$; TAG) single crystals by laser FZ method. *J. Cryst. Growth* **2005**, *275*, e663–e667. [CrossRef]
119. Sekijima, T.; Fujii, T.; Wakino, K.; Okada, M. Optical Faraday rotator using Ce-substituted fibrous YIG single crystal grown by floating zone method with YAG laser heating. In Proceedings of the 1999 IEEE MTT-S International Microwave Symposium Digest (Cat. No.99CH36282), Anaheim, CA, USA, 13–19 June 1999; Volume 3, pp. 1369–1372.
120. Singh, S.; Lal, B. Crystalline fiber of dye-doped L-arginine phosphate by the laser-heated pedestal growth technique. *J. Cryst. Growth* **2008**, *310*, 2039–2042. [CrossRef]
121. Singh, S.; Lal, B. Laser heated pedestal growth and characterization of the crystalline fibers of KDP doped L-arginine phosphate. *J. Cryst. Growth* **2010**, *312*, 443–446. [CrossRef]
122. Costa, F.M.; Ferreira, N.M.; Rasekh, S.; Fernandes, A.J.S.; Torres, M.A.; Madre, M.A.; Diez, J.C.; Sotelo, A. Very large superconducting currents induced by growth tailoring. *Cryst. Growth Des.* **2015**, *15*, 2094–2101. [CrossRef]
123. Ferreira, N.M.; Rasekh, S.H.; Costa, F.M.; Madre, M.A.; Sotelo, A.; Diez, J.C.; Torres, M.A. New method to improve the grain alignment and performance of thermoelectric ceramics. *Mater. Lett.* **2012**, *83*, 144–147. [CrossRef]
124. Silva, R.A.; Costa, F.M.; Silva, R.F.; Andreeta, J.P.; Hernandes, A.C. Electric field-modified segregation in crystal fibers of colossal magnetoresistive $La_{0.7}Ca_{0.3}MnO_3$. *J. Cryst. Growth* **2008**, *310*, 3568–3572. [CrossRef]
125. Costa, F.M.; Silva, R.F.; Vieira, J.M. Influence of epitaxial growth on superconducting properties of LFZ Bi-Sr-Ca-Cu-O fibres. Part I. Crystal nucleation and growth. *Physica C* **1997**, *289*, 161–170. [CrossRef]
126. Costa, F.M.; Silva, R.F.; Vieira, J.M. Diffusion phenomena and crystallization path during the growth of LFZ Bi–Sr–Ca–Cu–O superconducting fibres. *Supercond. Sci. Technol.* **2001**, *14*, 910–920. [CrossRef]
127. Costa, F.M.; Carrasco, M.M.; Silva, R.F.; Vieira, J.M. Chapter 2: High Tc superconducting fibers processed by conventional and electrical assisted laser floating zone. In *Perspectives on Superconductivity Research*; Lewis, P.S., Ed.; Nova Science Publishers: Hauppauge, NY, USA, 2007; pp. 35–59.
128. Carrasco, M.M.; Silva, R.F.; Vieira, J.M.; Costa, F.M. Pulling rate and current intensity competition in an electrically assisted laser floating zone. *Supercond. Sci. Technol.* **2009**, *22*, 065016. [CrossRef]
129. Constantinescu, G.; Rasekh, S.; Torres, M.A.; Madre, M.A.; Sotelo, A.; Diez, J.C. Improvement of thermoelectric properties in $Ca_3Co_4O_9$ ceramics by Ba doping. *J. Mater. Sci. Mater. Electron.* **2015**, *26*, 3466–3473. [CrossRef]
130. Vieira, J.M.; Silva, R.A.; Silva, R.F.; Costa, F.M. Enhancement of superconductivity in LFZ-grown BSCCO fibres by steeper axial temperature gradients. *Appl. Surf. Sci.* **2012**, *258*, 9175–9180. [CrossRef]
131. Andreeta, M.R.B.; Andreeta, E.R.M.; Hernandes, A.C.; Feigelson, R.S. Thermal gradient control at the solid–liquid interface in the laser-heated pedestal growth technique. *J. Cryst. Growth* **2002**, *234*, 759–761. [CrossRef]
132. Carrasco, M.F.; Silva, R.A.; Silva, N.J.O.; Silva, R.F.; Vieira, J.M.; Costa, F.M. Radial inhomogeneities induced by fiber diameter in electrically assisted LFZ growth of Bi-2212. *Appl. Surf. Sci.* **2009**, *255*, 5503–5506. [CrossRef]
133. Costa, F.M.; Silva, R.F.; Vieira, F.M. Phase transformation kinetics during thermal annealing of LFZ Bi-Sr-Ca-Cu-O superconducting fibers in the range 800–870 °C. *Physica C* **1999**, *323*, 23–41. [CrossRef]

134. Carrasco, M.F.; Amaral, V.S.; Silva, R.F.; Vieira, J.M.; Costa, F.M. Annealing time effect on Bi-2223 phase development in LFZ and EALFZ grown superconducting fibres. *Appl. Surf. Sci.* **2006**, *252*, 4957–4963. [CrossRef]
135. Sotelo, A.; Madre, M.A.; Diez, J.C.; Rasekh, S.; Angurel, L.A.; Martínez, E. The influence of Pb and Ag doping on the Jc(H, T) dependence and the mechanical properties of Bi-2212 textured rods. *Supercond. Sci. Technol.* **2009**, *22*, 034012. [CrossRef]
136. Madre, M.A.; Costa, F.M.; Ferreira, N.M.; Costa, S.I.R.; Rasekh, S.; Torres, M.A.; Diez, J.C.; Amaral, V.S.; Amaral, J.S.; Sotelo, A. High thermoelectric performance in $Bi_{2-x}Pb_xBa_2Co_2O_y$ promoted by directional growth and annealing. *J. Eur. Ceram. Soc.* **2016**, *36*, 67–74. [CrossRef]
137. Terasaki, I.; Sasago, Y.; Uchinokura, K. Large thermoelectric power in $NaCo_2O_4$ single crystals. *Phys. Rev. B* **1997**, *56*, R12685(R). [CrossRef]
138. Fergus, J.W. Oxide materials for high temperature thermoelectric energy conversion. *J. Eur. Ceram. Soc.* **2012**, *32*, 525–540. [CrossRef]
139. Funahashi, R.; Matsubara, I.; Ikuta, H.; Takeuchi, T.; Mizutani, U.; Sodeoka, S. An oxide single crystal with high thermoelectric performance in air. *Jpn. J. Appl. Phys.* **2000**, *39*, L1127–L1129. [CrossRef]
140. Sun, N.; Dong, S.T.; Zhang, B.B.; Chen, Y.B.; Zhou, J.; Zhang, S.T.; Gu, Z.B.; Yao, S.H.; Chen, Y.F. Intrinsically modified thermoelectric performance of alkaline-earth isovalently substituted $[Bi_2AE_2O_4][CoO_2]y$ single crystals. *J. Appl. Phys.* **2013**, *114*, 043705. [CrossRef]
141. Constantinescu, G.; Rasekh, S.; Torres, M.A.; Madre, M.A.; Diez, J.C.; Sotelo, A. Enhancement of the high-temperature thermoelectric performance of $Bi_2Ba_2Co_2O_x$ ceramics. *Scr. Mater.* **2013**, *68*, 75–78. [CrossRef]
142. Madre, M.A.; Costa, F.M.; Ferreira, N.M.; Sotelo, A.; Torres, M.A.; Constantinescu, G.; Rasekh, S.; Diez, J.C. Preparation of high-performance $Ca_3Co_4O_9$ thermoelectric ceramics produced by a new two-step method. *J. Eur. Ceram. Soc.* **2013**, *33*, 1747–1754. [CrossRef]
143. Sotelo, A.; Rasekh, S.; Guilmeau, E.; Madre, M.A.; Torres, M.A.; Marinel, S.; Diez, J.C. Improved thermoelectric properties in directionally grown $Bi_2Sr_2Co_{1.8}O_y$ ceramics by Pb for Bi substitution. *Mater. Res. Bull.* **2011**, *46*, 2537–2542. [CrossRef]
144. Çetin Karakaya, G.; Özçelik, B.; Torres, M.A.; Madre, M.A.; Sotelo, A. Effect of Na-doping on thermoelectric and magnetic performances of textured $Bi_2Sr_2Co_2O_y$ ceramics. *J. Eur. Ceram. Soc.* **2018**, *38*, 515–520. [CrossRef]
145. Özçelik, B.; Çetin, G.; Gürsul, M.; Madre, M.A.; Sotelo, A.; Adachi, S.; Takano, Y. Low temperature thermoelectric properties of K-substituted $Bi_2Sr_2Co_2O_y$ ceramics prepared via laser floating zone technique. *J. Eur. Ceram. Soc.* **2019**, *39*, 3082–3087. [CrossRef]
146. Madre, M.A.; Rasekh, S.; Torres, M.A.; Bosque, P.; Diez, J.C.; Sotelo, A. Enhanced electrical and thermoelectric properties from textured $Bi_{1.6}Pb_{0.4}Ba_2Co_2O_y$/Ag composites. *J. Mater. Sci.* **2017**, *52*, 4833–4839. [CrossRef]
147. Rasekh, S.; Ferreira, N.M.; Costa, F.M.; Constantinescu, G.; Madre, M.A.; Torres, M.A.; Diez, J.C.; Sotelo, A. Development of a new thermoelectric $Bi_2Ca_2Co_{1.7}O_x$ + $Ca_3Co_4O_9$ composite. *Scr. Mater.* **2014**, *80*, 1–4. [CrossRef]
148. Ferreira, N.M.; Madre, M.A.; Torres, M.A.; Davarpanah, A.; Amaral, V.; Costa, F.M.; Sotelo, A. Improvement of grain alignment in $Bi_2Sr_2Co_{1.8}O_y$ thermoelectric through the electrically assisted laser floating zone. *Mater. Res. Bull.* **2020**, *130*, 110933. [CrossRef]
149. Pfann, W.G.; Wagner, R.S. Principles of field freezing. *Trans. Metall. Soc. AIME* **1962**, *224*, 1139–1146.
150. Wagner, R.S.; Miller, C.E.; Brown, H. Field-Freezing Experiments on Bi-Sn and Au-Ge Alloys. *Trans. TMS AIME* **1966**, *236*, 554–558.
151. Ohtaki, M. Recent aspects of oxide thermoelectric materials for power generation from mid-to-high temperature heat source. *J. Ceram. Soc. Jpn.* **2011**, *119*, 770–775. [CrossRef]
152. Wang, Y.; Rogado, N.S.; Cava, R.J.; Ong, N.P. Spin entropy as the likely source of enhanced thermopower in $Na_xCo_2O_4$. *Nature* **2003**, *423*, 425–428. [CrossRef]
153. Carreira, F.P.; Ferreira, N.M.; Kovalevsky, A.V. Laser processing as a tool for designing donor-substituted calcium manganite-based thermoelectrics. *J. Alloys Compd.* **2020**, *829*, 154466. [CrossRef]
154. Ferreira, N.M.; Neves, N.R.; Ferro, M.C.; Torres, M.A.; Madre, M.A.; Costa, F.M.; Sotelo, A.; Kovalevsky, A.V. Growth rate effects on the thermoelectric performance of $CaMnO_3$-based ceramics. *J. Eur. Ceram. Soc.* **2019**, *39*, 4184–4188. [CrossRef]
155. Ferreira, N.M.M.; Costa, F.M.; Kovalevsky, A.V.; Madre, M.A.; Torres, M.A.; Diez, J.C.; Sotelo, A. New environmentally friendly Ba-Fe-O thermoelectric material by flexible laser floating zone processing. *Scr. Mater.* **2018**, *145*, 54–57. [CrossRef]
156. Amaral, F.; Costa, L.C.; Valente, M.A.; Fernandes, A.J.S.; Franco, N.; Alves, E.; Costa, F.M. Colossal dielectric constant of poly- and single-crystalline $CaCu_3Ti_4O_{12}$ fibres grown by the laser floating zone technique. *Acta Mater.* **2011**, *59*, 102–111. [CrossRef]
157. Sergeenkov, S.; Cardoso, C.A.; Andreeta, M.R.B.; Hernandes, A.C.; Leite, E.R.; Araújo-Moreira, F.M. Growth and magnetic properties of bulk electron doped $La_{0.7}Ce_{0.3}MnO_3$ manganites. *Phys. Status Solidi A* **2011**, *208*, 1704–1707. [CrossRef]
158. Uda, S.; Tsubota, T. Ionic impurity transport and partitioning at the solid-liquid interface during growth of lithium niobate under an external electric field by electric current injection. *J. Cryst. Growth* **2010**, *312*, 3650–3657. [CrossRef]
159. Cherif, M.; Hicher, P.; Benamara, O.; Lebbou, K.; Haumont, R.; Duffar, T. Electric Field Effects During Solidification of the Ternary Oxide Eutectic Al_2O_3-YAG-ZrO_2. *Cryst. Res. Technol.* **2018**, *53*, 1700251. [CrossRef]
160. Qiao, G.W.; Zhang, J.S.; Huang, J.G.; Jiang, M.; Ge, Y.L.; Wang, Y.Z.; Hu, Z.Q. An investigation of melt-textured high T_c superconductor wires made by laser heated pedestal growth technique. *Physica C* **1989**, *162–164*, 907–908. [CrossRef]
161. Cima, M.J.; Flemings, M.C.; Figueredo, A.M.; Nakade, M.; Ishii, H.; Brody, H.D.; Haggerty, J.S. Semisolid solidification of high temperature superconducting oxides. *J. Appl. Phys.* **1992**, *72*, 179–190. [CrossRef]
162. Figueredo, A.M.; Cima, M.J.; Flemings, M.C.; Haggerty, J.S. Directional Phase Formation on Melting via Peritectic Reaction. *Metall. Mat. Trans. A* **1994**, *25*, 1747–1760. [CrossRef]

163. Figueredo, A.M.; Cima, M.J.; Flemings, M.C.; Haggerty, J.S.; Hara, T.; Ishii, H.; Ohkuma, T.; Hirano, S. Properties of $Ba_2YCu_3O_{7-\delta}$ filaments directionally solidified by the laser-heated floating zone technique. *Physica C* **1995**, *241*, 92–102. [CrossRef]
164. Feigelson, R.S.; Gazit, D.; Fork, D.K.; Geballe, T.H. Superconducting Bi-Ca-Sr-Cu-O fibers grown by the Laser-Heated Pedestal Growth Method. *Science* **1988**, *240*, 1642–1645. [CrossRef] [PubMed]
165. Sun, J.Z.; Feigelson, R.S.; Gazit, D.; Fork, D.; Geballe, T.H.; Kapinulnik, A. Properties of high-Tc oxide fibers from laser heated pedestal growth. *IEEE Trans. Magn.* **1989**, *25*, 2014–2016. [CrossRef]
166. De la Fuente, G.F.; Beltrán, D.; Ibáñez, R.; Martínez, E.; Beltrán, A.; Segura, A. Crystal fibers of Bi-Sr-Ca-Cu-O materials grown by the laser floating zone method. *J. Less Common Met.* **1989**, *150*, 253–260. [CrossRef]
167. De la Fuente, G.F.; Navarro, R.; Lera, F.; Rillo, C.; Bartolomé, J.; Badía, A.; Beltrán, D.; Ibáñez, R.; Beltrán, A.; Sinn, E. LFZ growth of (Bi, Pb)-Sr-Ca-Cu-O superconducting fibers. *J. Mater. Res.* **1991**, *6*, 699–703. [CrossRef]
168. Angurel, L.A.; de la Fuente, G.F.; Badía, A.; Larrea, A.; Díez, J.C.; Peña, J.I.; Martínez, E.; Navarro, R. Textured BSCCO superconductors obtained via laser induced directional solidification. In *Studies of High Temperature Superconductor*; Narlikar, A., Ed.; Nova Science Publishers: Hauppauge, NY, USA, 1996; Volume 21, pp. 1–31.
169. Carrillo-Cabrera, W.; Göpel, W.; de la Fuente, G.F.; Verdún, H.R. Preparation and growth of (Bi,Pb)-Sr-Ca-Cu-O superconductors. *Appl. Phys. Lett.* **1989**, *55*, 1032–1034. [CrossRef]
170. Snoeck, E.; Larrea, A.; Roucau, C.; de la Fuente, G.F.; Huang, Y. Microstructure of (Bi, Pb)-Sr-Ca-Cu-O fibers: Study by electron microscopy. *Physica C* **1992**, *198*, 129–136. [CrossRef]
171. Larrea, A.; Snoeck, E.; Badía, A.; de la Fuente, G.F.; Navarro, R. Microstructure, interfaces and magnetic behavior of thick Ag/BSCO composite fibres. *Physica C* **1994**, *220*, 21–32. [CrossRef]
172. Miao, H.; Díez, J.C.; Angurel, L.A.; Peña, J.I.; de la Fuente, G.F. Phase formation and microstructure of laser floating zone grown BSCCO fibers: Reactivity aspects. *Solid State Ion.* **1997**, *101–103*, 1025–1032. [CrossRef]
173. Gazit, D.; Feigelson, R.S. Laser-Heated pedestal growth of high T_c Bi-Sr-Ca-Cu-O superconducting fibers. *J. Cryst. Growth* **1988**, *91*, 318–330. [CrossRef]
174. Gazit, D.; Peszkin, P.N.; Moulton, L.V.; Feigelson, R.S. Influence of growth rate on the structure and composition of float zone grown $Bi_2Sr_2CaCu_2O_8$ superconducting fibers. *J. Cryst. Growth* **1988**, *91*, 545–549. [CrossRef]
175. De la Fuente, G.F.; Díez, J.C.; Angurel, L.A.; Peña, J.I.; Sotelo, A.; Navarro, R. Wavelength dependence on laser floating zone processing. A case study with Bi-Sr-Ca-Cu-O superconductors. *Adv. Mater.* **1995**, *7*, 853–856. [CrossRef]
176. Diez, J.C.; Angurel, L.A.; Miao, H.; Fernández, J.M.; de la Fuente, G.F. Processing of textured BSCCO superconductors by laser-induced directional solidification. *Supercond. Sci. Technol.* **1998**, *11*, 101–106. [CrossRef]
177. Angurel, L.A.; Díez, J.C.; Martínez, E.; Peña, J.I.; de la Fuente, G.F.; Navarro, R. Growth rate effects on thin $Bi_2Sr_2CaCu_2O_{8+\delta}$ textured rods. *Physica C* **1998**, *302*, 39–50. [CrossRef]
178. Natividad, E.; Díez, J.C.; Peña, J.I.; Angurel, L.A.; Navarro, R.; Andrés, J.M.; Ferrando, A.C. Correlation of radial inhomogeneities and critical current at 77 K in LFZ Bi-2212 textured thin rods. *Physica C* **2002**, *372−376*, 1051–1054. [CrossRef]
179. Natividad, E.; Díez, J.C.; Angurel, L.A.; Andrés, J.M. Successful application of simplex methods to the optimization of textured superconducting ceramics. *J. Am. Ceram. Soc.* **2004**, *87*, 1216–1221. [CrossRef]
180. Sotelo, A.; Mora, M.; Madre, M.A.; Díez, J.C.; Angurel, L.A.; de la Fuente, G.F. Ag distribution in thick Bi-2212 floating zone textured rods. *J. Eur. Ceram. Soc.* **2005**, *25*, 2947–2950. [CrossRef]
181. Özcelik, B.; Nane, O.; Sotelo, A.; Madre, M.A. Effect of Yttrium substitution on superconductivity in Bi-2212 textured rods prepared by a LFZ technique. *Ceram. Int.* **2016**, *42*, 3418–3423. [CrossRef]
182. Özcelik, B.; Ergin, I.; Madre, M.A.; Sotelo, A. Effect of Rubidium substitution on the physical and superconducting properties of textured High-Tc BSCCO samples. *J. Supercond. Nov. Magn.* **2020**, *33*, 1285–1292. [CrossRef]
183. Ergin, I.; Özcelik, B.; Madre, M.A.; Sotelo, A. Effect of Cesium substitution on the superconducting properties of Bi-2212 samples prepared via solid-state reaction and laser floating zone technique. *J. Supercond. Novel Magn.* **2019**, *32*, 3439–3448. [CrossRef]
184. Natividad, E.; Mora, M.; Díez, J.C.; Peña, J.I.; García, M.; Angurel, L.A.; Navarro, R. Coaxial configuration of Bi-2212 textured ceramics: A possibility for improved current leads. *IEEE Trans. Appl. Supercond.* **2001**, *11*, 2559–2562. [CrossRef]
185. Angurel, L.A.; Díez, J.C.; de la Fuente, G.F. Laser induced cylindrical zone melting of $Bi_2Sr_2CaCu_2O_{8+\delta}$ superconductors. *Z. Anorg. Allg. Chem.* **2009**, *635*, 1767–1772. [CrossRef]
186. Costa, F.M.; Carrasco, M.F.; Ferreira, N.; Silva, R.F.; Vieira, J.M. LFZ fibre texture modification induced by electrical polarization. *Physica C* **2004**, *408−410*, 915–916. [CrossRef]
187. Carrasco, M.F.; Silva, R.A.; Silva, R.F.; Amaral, V.S.; Costa, F.M. Critical Current Density Improvement in BSCCO Superconductors by Application of an Electric Current during Laser Floating Zone Growth. *Physica C* **2007**, *460−462*, 1347–1348. [CrossRef]
188. Mora, M.; Martínez, E.; Angurel, L.A.; Navarro, R. Electrical dc characteristics of textured BSCCO-2212 thin rods developed for current leads. *IEEE Trans. Appl. Supercond.* **1999**, *9*, 2343–2346. [CrossRef]
189. García-Tabarés, L.; Calero, J.; Abramian, P.; Toral, F.; Grau, A.; Angurel, L.A.; Díez, J.C. Study of superconducting to normal transition propagation in BSCCO2212 fibers. *IEEE Trans. Appl. Supercond.* **1999**, *9*, 1880–1883. [CrossRef]
190. García-Tabarés, L.; Calero, J.; Abramian, P.; Toral, F.; Angurel, L.A.; Díez, J.C.; Burriel, R.; Natividad, E.; Iturbe, R.; Etxeandía, J. Design, fabrication and tests of a 600 A HTc current lead for the LHC correction magnets. *IEEE Trans. Appl. Supercond.* **2001**, *11*, 2543–2546. [CrossRef]

191. Angurel, L.A.; Bona, M.; Andrés, J.M.; Muñoz-Rojas, D.; Casañ-Pastor, N. High quality silver contacts on ceramic superconductors obtained by electrodeposition form non-aqueous solvents. *Supercond. Sci. Technol.* **2005**, *18*, 135–141. [CrossRef]
192. Rey-García, F.; Ferreira, N.M.; Fernandes, A.J.S.; Costa, F.M. Processing of the Nd_2O_3:SiO_2 system by Laser Floating Zone in air. *Results Phys.* **2020**, *17*, 103180. [CrossRef]
193. Andreeta, M.R.B.; Hernandes, A.C.; Cuffini, S.L.; Guevara, J.A.; Mascarenhas, Y.P. Laser heated pedestal growth of orthorhombic $SrHfO_3$ single crystal fiber. *J. Cryst. Growth* **1999**, *200*, 621–624. [CrossRef]
194. Lim, H.J.; DeMattei, R.C.; Feigelson, R.S.; Rochford, K. Striations in YIG fibers grown by the laser-heated pedestal growth. *J. Cryst. Growth* **2000**, *212*, 191–203. [CrossRef]
195. Chen, J.C.; Chen, C.Y. Growth of $Ba_{1-x}Ca_xTiO_3$ single-crystal fibers by a laser heated pedestal method. *J. Cryst. Growth* **2002**, *236*, 640–646. [CrossRef]
196. Weiner, A.M. *Ultrafast Optics*; John Wiley & Sons: Hoboken, NJ, USA, 2009.
197. Dausinger, F.; Lichtner, F.; Lubatschowski, H. *Femtosecond Technology for Technical and Medical Applications*; Springer: Cham, Switzerland, 2004.
198. Ebrahim-Zadeh, M.; Sorokina, I.T. *Mid-Infrared Coherent Sources and Applications*; Springer: Cham, Switzerland, 2008.
199. Malinauskas, M.; Zukauskas, A.; Hasegawa, S.; Hayasaki, Y.; Mizeikis, V.; Buividas, R.; Juodkazis, S. Ultrafast laser processing of materials: From science to industry. *Light Sci. Appl.* **2016**, *5*, e16133. [CrossRef] [PubMed]
200. Sheperd, D.P.; Choudhary, A.; Lagatsky, A.A.; Kannan, P.; Beecher, S.J.; Eason, R.W.; Mackenzie, J.I.; Feng, X.; Sibbett, W.; Brown, C.T.A. Ultrafast high-repetition-rate waveguide lasers. *IEEE J. Sel. Top. Quantum Electron.* **2016**, *22*, 1100109.